ELECTROWETTING ON DIELECTRIC DIGITAL MICROFLUIDICS FOR 3-DIMENSIONAL CELL CULTURE AND CHEMICAL SCREENING

by

SUBIN MAC GEORGE

Presented to the Faculty of the Graduate School of

The University of Texas at Arlington in Partial Fulfillment

of the Requirements

for the Degree of

DOCTOR OF PHILOSOPHY

THE UNIVERSITY OF TEXAS AT ARLINGTON

December 2014

Acknowledgements

I would like to acknowledge first and foremost, the guidance and mentoring of my advisor Professor Hyejin Moon. More than just allowing me to carry out research in her lab, she invested her time and effort in me and trained me to think like a researcher. I am thankful for her patience and encouragement and the life lessons that she has imparted to me over our years of interaction.

I would also like to thank my committee members Dr. Albert Tong, Dr. Ankur Jain, Dr. Alan Bowling, and Dr. Yi Hong for their time, interest and helpful comments.

I collectively thank all my lab members, past and present, at the Integrated Micro and Nanofluidic Systems Lab. They have always been willing to offer their support, insights and encouragement and have crossed over the bridge from colleagues to friends.

I am grateful to my parents for the educational opportunities and support that they have provided me with. Lastly, I would like to recognize the constant support and encouragement that my wife Nisha has been, without whom this achievement would have been impossible. Thank you for your support, understanding and companionship through all the years.

November 7, 2014

Abstract

ELECTROWETTING ON DIELECTRIC DIGITAL MICROFLUIDICS FOR 3-DIMENSIONAL CELL CULTURE AND CHEMICAL SCREENING

Subin Mac George, PhD

The University of Texas at Arlington, 2014

Supervising Professor: Hyejin Moon

Microfluidic devices have allowed improved cell culture studies to be carried out by allowing greater spatiotemporal control over the cell environment while at the same time providing greater throughput, increased automation capabilities and reagent savings. To improve the relevancy of such studies, 3-dimensional (3D) cell culture has been attempted in microfluidic devices. 3D cell culture is known to better mimic and recreate the environment that cells in the body experience as compared to conventional 2-dimensional cell culture. However, incorporating 3D cell culture into conventional channel based microfluidic devices have proven to be challenging. Hydrogels which provide the 3D environment in microfluidic devices are prone to clog up microfluidic channels or break up due to excess pressure, thereby necessitating greater controls and complication of conventional channel based microfluidic devices.

Electro-wetting on dielectric (EWOD) digital microfluidic (DMF) is another alternative microfluidic platform that is proposed to counter these problems. Since EWOD DMF flow occurs through discrete droplets without requiring channels, delicate gels can be handled without compromising the microfluidic device integrity or gel integrity. In addition, EWOD DMF has already been shown to be an efficient platform for multiplexing and liquid delivery.

This study investigates the feasibility of EWOD DMF for 3D cell culture. To do this, an alginate hydrogel is employed and alginate gelation on EWOD DMF is investigated. Various designs to allow for reliable hydrogel formation are examined and an optimal design is developed. Using this design, an EWOD DMF device is developed which is capable of forming cell seeded alginate hydrogels, diluting and delivering a chemical species at different concentrations to the hydrogels and examining the effect of delivered chemicals on the 3D cultured cells. Thus, this proof of concept device demonstrates how EWOD DMF can be used for integrated 3D cell culture and chemical screening.

Table of Contents

List of Illustrations

Chapter 1

Introduction to Microfluidic Cell Culture

Microfluidics deals with the study and manipulation of fluids whose characteristic length is at the micrometer scale. It has been an emerging field of study over the last two decades and has now matured into a multi-faceted discipline which encompasses a wide variety of methods by which fluids at the micro scale can be manipulated.

One area in which microfluidics has found increasing applications is in the field of cell biology, where there has been greater interest in studying cell behavior and response at the microscale level. Current macroscale based approaches, though useful in their own regards, do not allow for the same level of control over cellular conditions and environments that microscale approaches can accomplish. At the same time, microfluidics also allows for increased miniaturization. This provides several benefits including reagent savings, faster reaction times, greater automation capabilities, as well as the ability to conduct a greater number of replicate experiments.

Cell culture using microfluidics has been the first proving grounds for biologists in order to demonstrate the feasibility of using microfluidics for cell based applications. The ability to culture cells in microfluidic devices presents specific advantages over conventional petri dish or multi well plate culture, since microfluidics allows for very precise spatial and temporal control over the cell microenvironment. This ability to greatly control the cell microenvironment leads to better controlled experiments and the ability to observe cell reactions to specific changes in their environments in a manner that was never possible using conventional cell culture and assay methods. With advances in cell biology, the benefits of 3-dimensional (3D) based cell culture over conventional 2-dimensional (2D) cell culture have become apparent, especially in regard to cell

morphology and physiology [1,2] resulting in a greater number of recent papers focusing on microfluidic 3D cell based culture and assays.

The miniaturization ability, automation benefits and reagent savings of microfluidics have been powerful incentives for the adoption of microfluidic devices towards drug development and screening, which have currently realized their miniaturization potential using existing high throughput screening (HTS) methods. Although various groups have looked to adapt microfluidics to work in conjunction with automated liquid handlers that are part of current HTS system components in attempts to increase miniaturization [3–5], there is a greater movement towards developing integrated microfluidic systems that can generate various concentrations of new chemical entities or drug candidates and deliver them to cell cultures in the form of assays.

1.1 Continuous Microfluidic Based Cell Culture

Most of the early research in microfluidics took place in the field of continuous microfluidics. Continuous microfluidics are characterized by the flow of a continuous phase of fluid (as opposed to a dispersed phase) through microscale channels. Since the evolution of microfluidics, flow has traditionally been envisioned as always being driven by a pressure difference. To maintain the pressure difference, a constrained geometry is required which usually takes the form of microchannels. Various pumping mechanisms have been developed over the years along with different methods of creating and integrating micro valves or other flow regulation controls to initiate and control the flow within the microchannels [6,7].

1.1.1 2D Cell Culture Using Continuous Microfluidics

Microfluidic cell culture in continuous microfluidics employs a basic format that comprises of a cell culture chamber which is accessible through fluidic pathways which allow for cell seeding, delivery of culture media to sustain the cells, delivery of reagents to affect cell behavior or to fluorescently label features of interest, and removal of waste media. Many microfluidic cell culture devices have been designed around this basic principle[8–12]. Long term culture (> 2 weeks) of cells has been demonstrated on these devices [13–16].

Since perfusion flow applies shear stress over cells that are being cultured, the method in which flow is introduced to the culture chamber is important. Most devices have the culture chamber in line with the fluidic channels. In order to decrease the shear stress, the depth of the culture chamber can be greater than the fluidic pathways so that they are shielded from the higher flow velocities. Other methods include isolating the culture chamber from bulk flow by placing culture chambers perpendicular to the bulk flow direction, or by increasing fluidic resistance to the culture chamber so that flow velocity at the culture chamber is decreased, resulting in more physiologically similar shear.

Lee, Hung et al [17] developed a microfluidic microbioreactor array in which they incorporated a protective C shaped ring to isolate the cultured cell from the high shear of fluid flow arriving at the cell chamber through the microchannel. A 2μm opening at the base of the C ring allowed media to perfuse gently into the culture chamber thereby mimicking physiological tissue conditions.

Zhang et al [18] developed a microfluidic device that not only cultured cells but also passaged them, as shown in Figure 1-1. This was done by the use of built in micro-sieves within the culture chambers that trapped cells during the cell seeding stage. These

cells multiply and grow and when confluency is reached, they are trypsinized and collected at the outlet. Cells that remained trapped in microsieves after trypsinization serve to seed the chambers for subsequent on-chip culturing thereby allowing multiple cycles of cell culture.

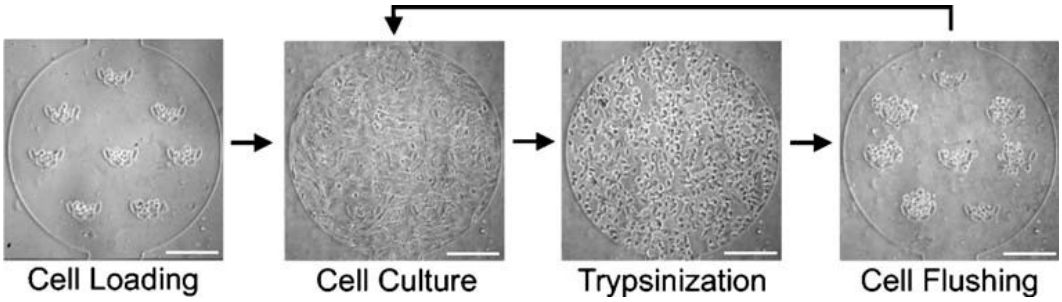

Figure 1-1 Microfluidic device showing continuous cell culture of BALB/3T3 as four steps; cell loading, cell culture, trypsinization, and cell flushing. Scale bar, 200 μm. Image taken from [18]

Liu et al [19] demonstrated another approach to culturing and passaging cells in a microfluidic device. Passaging was enabled by using a PDMS flexible diaphragm to apply hydrodynamic shear force, which detached a fraction of the passaged cancer cells from the surface to be used as output, while the remaining attached cells served for reuse in subsequent cultures. Using this approach, they demonstrated cell viability over 30 days of continuous culture and 9 passages.

Apart from passaging and basic culture of cells, microfluidic cell culture devices are used to observe the interactions of cells with the microenvironment [20]. The effects of shear force on cell functionality, arrangement and morphology in microfluidic cell culture systems have been demonstrated [21–24]. The effect of cell adhesive and cell repellant micropatterns on the differentiation of muscle cells has been demonstrated by Tourovskaia et al [16].

VanDersarl et al [25] came up with a microfluidic architecture which decoupled signal delivery from direct fluid flow over cells, thereby allowing for spatial and temporal control over signal delivery over large culture areas. This was achieved by separating cell culture wells from direct fluid flow by means of a nanoporous membrane which allowed chemical signals to diffuse through and reach the cells that were being cultured on the membrane. This approach was applied by Kawada et al [26] to demonstrate the effect of spatiotemporal control on stem cell differentiation.

As the number of cell culture chambers increase, the complexity of the design also tends to increase as seen in Figure 1-2**Error! Reference source not found.**, since a larger number of control valves and fluidic pathways will be required. This becomes even further complicated if individual access to culture chambers is required to allow for greater control over cell conditions without fear of cross contamination [27].

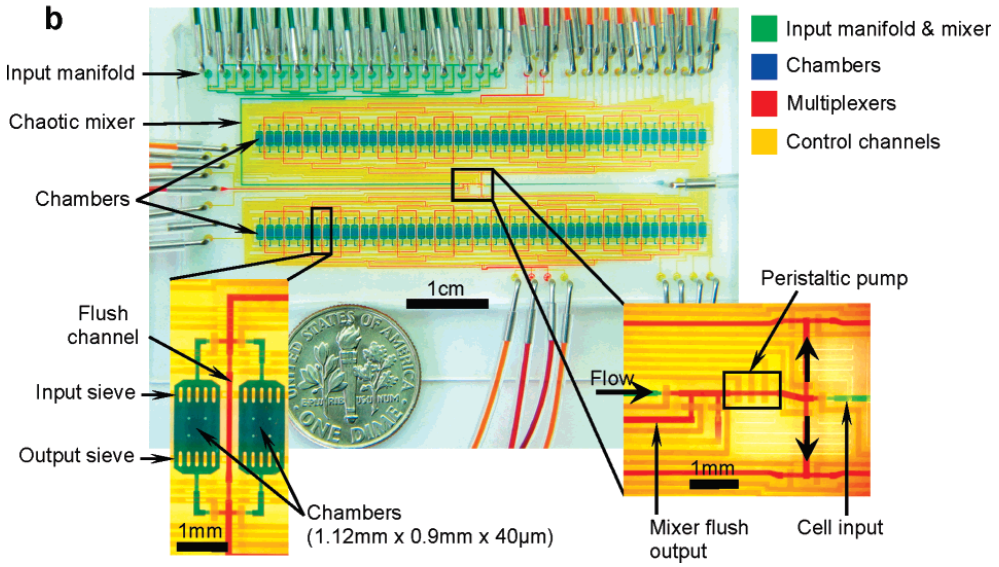

Figure 1-2 Complexity of connections increase with upscaling of continuous microfluidic devices as seen in this picture of a cell culture chip. Left inset shows details of two culture chambers with the multiplexer flush channel in between them. The right inset shows the root of the input multiplexer, with the peristaltic pump, a waste output for flushing the mixer, and the cell input line. Image taken from reference [6].

1.1.2 3D Cell Culture Using Continuous Microfluidics

Conventional in vitro cell studies used to rely on 2-dimensional (2D) cell culture, but cells in vivo grow in 3 dimensions (3D) and are surrounded by other cells as well as the extra cellular matrix. These cell-cell and cell-matrix interactions that occur in vivo are not replicated in 2D in vitro experiments and thus, there is a discernible difference in the morphology and physiology of cells grown in 2D when compared to cells in vivo [28]. This is schematically represented in Figure 1-3. As 3D cell culture gains more and more prominence as a means to more accurately capture cell behavior, various research groups have tried to adapt microfluidic 2D cell culture devices towards 3D cell culture. The main challenge in this adaptation is the means of creating a 3D microenvironment in which the cells can be cultured.

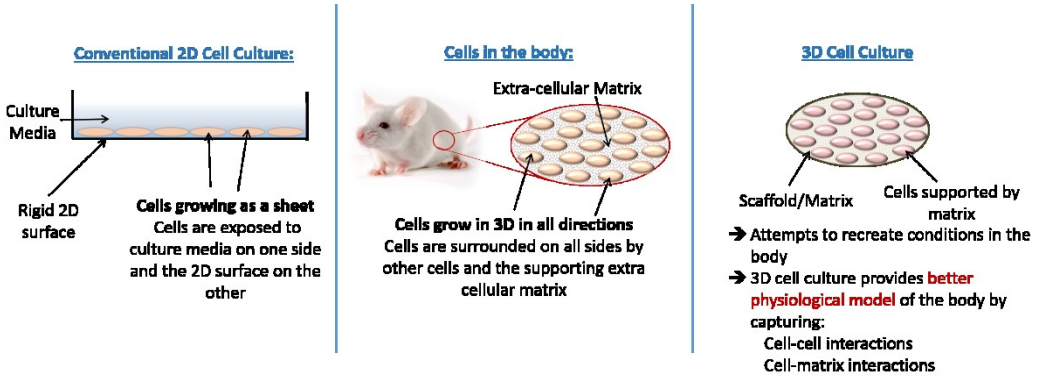

Figure 1-3 Schematic of difference in environment between 2D cell culture, cells in the body and 3D cell culture. Since 3D cell culture attempts to recreate the environment in the body, using 3D cell culture in experiments and cell studies allows more relevant information to be obtained.

Attempts to create suitable 3D environments have focused on encapsulating cells in hydrogels [29–31]. Hydrogels used in continuous microfluidics need to be anchored to prevent the gels from being pushed through the microfluidic circuit during perfusion. Anchoring is done in most of the papers discussed by allowing the gelation of

the hydrogel to occur on microposts or micropillars as demonstrated in Figure 1-4. at the targeted cell culture sites [32–34]. Since the gelation of the hydrogel can obstruct fluidic pathways, various approaches have been attempted to control when and where gel formation occurs. The simplest approach for 3D cell culture involves using a needle to directly inject cell laden hydrogel into the target cell culture site [33–35]. This eliminates the possibility of gel forming happening elsewhere and clogging the system. Such approaches, though simple to implement, require more manual operation and preparation and take away from the automation benefits of microfluidics.

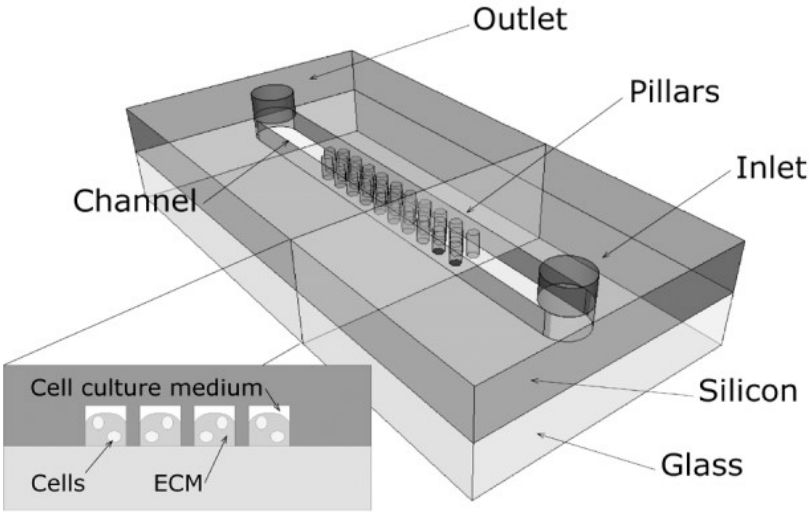

Figure 1-4 Conceptual image of chip for 3-D cell culture in extracellular matrix. Typical dimensions: channel width 400 µm, channel depth 90 µm, pillar diameter 40 µm, spacing/pitch 20–70 µm. Cross-cut shows center of chip. Image taken from [32]

One approach to circumvent the extra manual assembly of the approach described earlier was described by Chen et al [36]. Here, a cell seeded alginate hydrogel is formed by the diffusion of Ca^{2+} ions into cell seeded alginate gel precursor, when both are flowed through 2 parallel streams. Once gel formation is complete, regular perfusion

can be done by replacing the Ca^{2+} stream with the desired reagent (culture media, fluorescent dye, etc.)

Kim et al [37] demonstrated another approach where hydrodynamic focusing was used to create a cell laden hydrogel. In this method, a cell seeded peptide hydrogel precursor is focused into the middle of a microfluidic channel by means of a sheath flow of distilled water, and then gelation is allowed to occur. This allows for controlled formation of the hydrogel within the middle of the device while still allowing for media to flow around the hydrogel to sustain the cells within the gel.

Lii et al [38] devised a microfluidic device for culturing cells in 3D which had a 4x4 array of culture chambers, each of which was individually addressable through a system of pneumatic valves. By flowing flowing cell seeded Matrigel through the fluidic network, cell seeded gel was introduced into the culture chambers. Then, by isolating each chamber from the main flow pathways by using microvalves, culture media was flushed through the system, thereby purging the fluidic channels of any residual gel. Following this step, the cell seeded Matrigels which are now located only in the culture chambers were allowed to polymerize. In order to apply higher perfusion rates to the cell seeded tissue constructs in the culture chambers without affecting the integrity of the hydrogels, Lii's design also incorporated ring shaped valves on top of the culture chamber as well as microposts at its exit. By actuating the valves, the volume of the chamber could be artificially reduced. Thus, by allowing the gel to polymerize in the reduced volume chamber while the valves were actuated, and then releasing the valves so that the chamber regained its original volume, a pathway for fluid to flow above the gel was created. This allowed for higher perfusion rates of upto 100μL/min to be applied without affecting the integrity of the gel posts or flushing them out of the culture chambers.

Using hydrogels in continuous microfluidic devices presents unique challenges because of the chance of clogging of microfluidic pathways by the hydrogels that leads to device failure. To avoid the complexities of using hydrogels, but still obtain 3D cell culture capabilities, Toh et al [39] presented a microfluidic based 3D mammalian cell perfusion-culture system. A micropillar array placed in a microfluidic channel was used to trap cells and then a binding agent was used to form a thin layer of matrix around the cells, resulting in the creation of a 3D environment for cells. Medium flow around the cells contained in the micropillars help to maintain in-vivo like perfusion, and combined with the ability to culture cells in 3D without using hydrogels, this approach has been adopted by various other papers [40–42] for gel free 3D cell culture.

Multi-cellular spheroids also present another method in which the benefits of 3D cell culture can be obtained without resorting to hydrogels. Conventional macroscale methods to culture spheroids use the hanging drop method, liquid overlay technique or the gyratory rotation technique [43] .

One approach to spheroidal cell culture is by using specially designed microwells in the path of microchannels as described by Ziółkowska et al [44] Here, cells are seeded in the entire device, and cells settle into microwells and form spheroids while the remaining cells in the channels can be washed away. This method, while easy to implement, requires careful control over cell seeding density since too low a density can result in multiple small aggregates per well, while too high can cause clogging of the system. This method however results in wastage of cells and lack of control over the size of spheroids.

Agastin et al [43] improved upon this method to allow for simpler operation and better control over spheroid size. This was done by fabricating microbubbles in a PDMS layer which was later functionalized and then bonded to a flow chamber. Colo205 cells

which were seeded in the device would roll along the surface and get trapped in the microbubbles wherein they would organize and aggregate into spheroids. Such a method allowed easy control over the size of the spheroids just by controlling the seeding solution's cell density.

Ota & Miki[45] presented another approach to culturing spheroids and controlling their size. This was done by creating a microrotational flow inside microchambers which caused cells to collect at the center of the microchamber, where they aggregated and formed into spheroids. Here also, size control can be obtained by adjusting the cell density of the seeding solution.

It can be clearly seen that many approaches have been taken to adapt cell culture to conventional continuous microfluidic devices but none have led to the adoption of a standardized platform that can be practically used for general 2D or 3D studies.

1.2 Electrowetting on Dielectric Digital Microfluidics Based Cell Culture

In electrowetting on dielectric (EWOD) digital microfluidics (DMF), discretization of picoliter- to microliter-sized droplets and their motion are individually controlled by applying external electric fields to the designated electrodes within the device. The principle of EWOD and the theory of droplet actuation have been covered in previous papers [46–48] and is covered in further detail in chapter 2.1. EWOD DMF device fabrication and the methods by which droplets are dispensed from a reservoir, transported, mixed and split have also been presented in literature [49] . Various applications including chemical [50] and enzymatic reactions [51], immunoassays [52–54], PCR [55,56], clinical diagnostics [57,58] and proteomics [59–62] have been reported. Since the compartmentalization (e.g. creating discretized droplet) and their motion on the surface (i.e. pumping of liquids) are solely done by electric field application, intricate

systems to drive and regulate flow such as pumps and valves are not required in a EWOD DMF. The elimination of these mechanical components (pumps and valves), which are more prone to failure, makes the devices much more robust and enables a true miniaturized fluidic platform. Another beneficial feature of EWOD DMF is that EWOD devices are not constrained by fluidic channels; liquid motion and pathways are guided by the electrode layout only. Thus, EWOD DMF presents itself with a reconfigurable mode of usage and a well-designed EWOD DMF device can be used for multiple applications instead of being limited to one application per device. Also, the integration of electronic components (be it resistance heaters, sensors, etc.) is less of a problem with EWOD DMF when compared to other type of microfluidic devices. Greater reagent savings are also realized in EWOD DMF over continuous microfluidics since there is no dead volume (which is the volume of the fluid in the fluidic pathways that is not usable).

1.2.1 2D Cell Culture Using EWOD DMF

Since EWOD DMF does not require encapsulation for its operation and can operate in air, it is more versatile and can find a larger range of applications than channel based droplet microfluidics. This is especially true for cell based applications, where the availability of oxygen and the oxygen gradient become significant for cell viability. Sugiura et al [63] reported their findings regarding channel based microfluidics, about how oxygen supply through oxygen permeable walls was more critical for cell culture than oxygen supply through static and perfusion medium. In EWOD DMF since drops are surrounded by air and walls are non-existent, the diffusion of oxygen and oxygen availability to cells in droplets is not a concern as it is in channel based continuous and digital microfluidics.

Also with regards to cell based bio applications, concerns about cross contamination between different cells and reagents, which exist in continuous microfluidics, are minimized in EWOD DMF since each drop can be considered to be a unique bioreactor.

One of the main challenges in adopting EWOD DMF for biological applications is the prevention of biofouling. Biofouling in EWOD DMF occurs when proteins (which are commonly found in biological materials) adsorb onto the hydrophobic surface, rendering it hydrophilic. The loss of hydrophobicity of the EWOD surface greatly limits further droplet actuations and needs to be avoided for reliable device operations. Various techniques have been attempted to limit biofouling, and common methods involve either encapsulating the droplets in oil media [64], or by using surfactants such as pluronic block polymers which inhibit protein adsorption [65,66].

Since EWOD DMF achieves drop motion by the use of voltage driven surface change, no actual electricity passes through the droplets. Air encapsulated droplet motion can be obtained by using voltages in the range of 100 V and AC frequencies of the order of 1 KHz. These voltages have been shown to be successful in droplet translation without having an adverse effect on cell viability. Although voltages can be reduced by using oil encapsulated system, such methods are generally not preferred while handling live cells since they limit oxygen diffusion as well as the type of reagents that can be handled.

In order for EWOD DMF to be considered for cell based applications, it is important to first demonstrate the compatibility of the system with live cell handling. This was first demonstrated by Barbulovic-Nad et al [67] who demonstrated the ability of EWOD DMF to manipulate and analyze cells. They first modeled the effects of EWOD electric field application on cells and concluded that even when applying 100 V between the top and bottom electrodes, the potential drop was of the order of 10-8 V and would

not have a measurable effect on cell viability. They confirmed this by transporting cell laden suspensions at different cell concentrations and then culturing the transported cells for 2 days externally without any significant cell death. They used their device to conduct a cytotoxicity assay solely through the use of EWOD DMF. Cell seeded droplets were introduced in reservoirs from which cell containing daughter droplets were dispensed. These cell containing droplets were transported on chip and then mixed with the cytotoxic agent at different concentrations, incubated, and then mixed with fluorescent dyes followed by further incubation and then imaging using a fluorescence plate reader. Their cell assay results indicated ~ 20 fold increase in sensitivity over macroscale experiments.

Concerns about the effect of the applied electric field on cell viability, the ability of drops to retain cells and transport them without allowing them to sediment or leave behind any reside, and the effects of Joule heating if any, on cells were also answered by Son and Garrell [68]. They used a EWOD DMF device to move and transport live yeast cells and zebrafish embryo using droplets and confirmed that the cells thus moved were viable and compatible with the EWOD DMF system. Au et al [69] expanded on this to demonstrate not only live cell transportation, but also culturing of bacteria, yeast and algae on a specially designed EWOD DMF based bioreactor. Continuous mixing of cells in suspension was done at regular intervals through EWOD actuation to ensure uniform distribution of gases, nutrients and cells in the cell suspended drop. From this parent drop, daughter drops containing cells were periodically dispensed and transported to designated electrodes from where an integrated plate reader took absorbance measurements so as to estimate the growth rates and density of cells. The growth rates of cells on the microfluidic device were shown to be comparable to growth rates at the macroscale and the ability to culture cells for upto 5 days was demonstrated. This device

was also used to perform a viability assay and genetic transformation to showcase the ability of EWOD DMF to integrate multiple processes onto a single platform.

Culture of adherent mammalian cells has also been done by using EWOD DMF. The key challenge in culturing adherent cells on DMF platforms is getting cells in suspension to deposit onto designated culture sites. The normal EWOD surface is hydrophobic and not favorable for cell attachment. However, several strategies have been demonstrated to circumvent this problem. Barbulovic-Nad et al [70] were the first to develop a method for adherent cell culture by coating target cell culture sites with ECM proteins like fibronectin to form hydrophilic adhesion pads. When droplets containing cell suspensions were placed over the adhesion pads, cells would settle down and attach to them. These adhesion pads not only served as culture sites for cells, but also enabled passive dispensing of reagents to the culture site. The hydrophilic adhesion pads always retained liquid over it, even when liquid was passed over the electrode containing the adhesion pad. This allowed for the replenishment of culture media without requiring any active means of dispensing. Also, when cells reached confluence, trypsin could be delivered to the culture sites by means of passive dispensing, which would cause cells to be dislodged. Further delivery of culture media to the culture site would block further trypsin digestion, and also carry cells in suspension to the next culture site. This method is shown below in Figure 1-5. Using this method, cells could be repeatedly passaged up to 4 times and culturing of 2 different cell types (CHO-K1 and HeLa) was demonstrated for as long as 8 days.

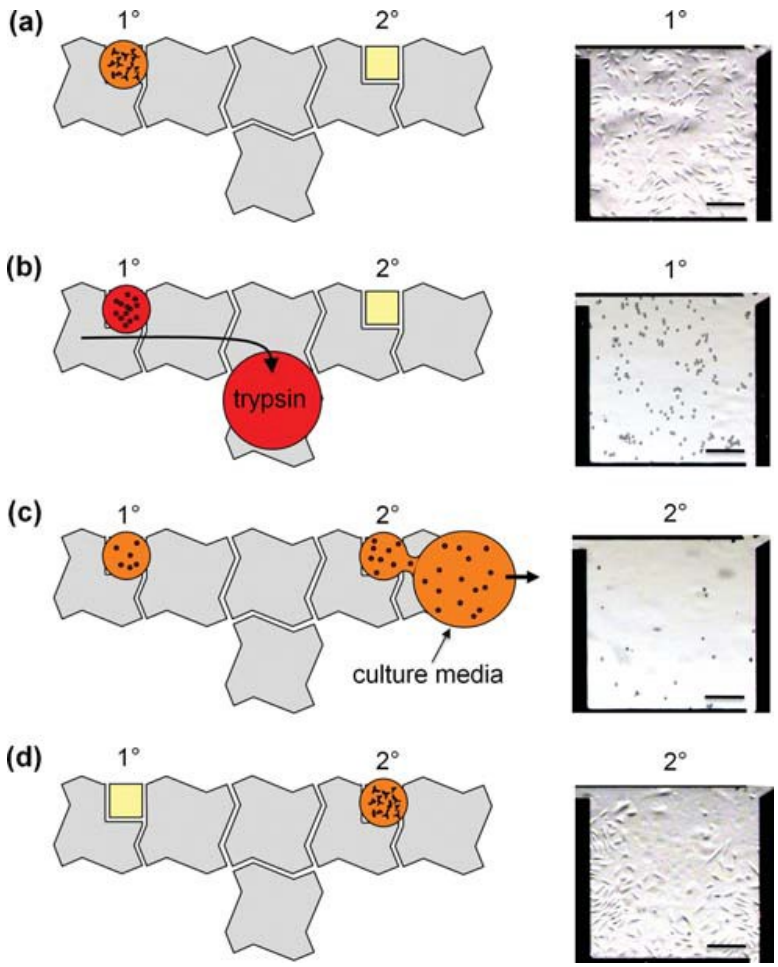

Figure 1-5 Schematic and pictures depicting subculture of CHO-K1 cells in droplets by digital microfluidics. (a) Monolayer of the first generation of cells on the primary (1˚) adhesion pad. (b) Cells dissociating from the surface of the 1˚ pad after delivery of trypsin. (c) Trypsinized cells being harvested in a droplet of media containing serum, and then seeded on the secondary (2 ˚) pad. (d) Monolayer of subcultured cells on the 2 ˚pad after 72 h. Scale bars are 200 mm. Image from [70]

This method was extended by Srigunapalan et al to demonstrate how primary cell culture could also be carried out using EWOD DMF [71].

Witters et al [72] demonstrated an improved method of creating hydrophilic sites by patterning the hydrophobic Teflon layer of the EWOD device by using a dry lift-off method. This method allowed for the creation of finely patterned hydrophilic sites whose

geometries and dimensions could be specified, thereby allowing cells to be arrayed as cell clusters or as single cells. Cells could be cultured on the patterned hydrophobic sites by using the principle of passive dispensing as described earlier.

Eydelnant et al [73] presented a passive method which they called “virtual microwells” for dispensing reagents on EWOD DMF by the Teflon lift off based hydrophilic patterning of sites on the DMF cover slip and applied it to DMF cell culture as a potential application. By using an impedance sensing system, Shih et al [74] was able to obtain feedback control and increasingly reliable droplet operation on EWOD DMF. By combining this with virtual microwells to carry out cell culture, they demonstrated how this system was also capable of measuring cell impedance which in turn could provide information on cell density and proliferation rates.

Cell based assays have also been performed and demonstrated on EWOD DMF [67,75–77]. EWOD digital microfluidics has also been used as a means to study specific cellular responses and behavior as demonstrated by Park et al in using EWOD digital microfluidics to characterize different cryoprotective agent mixtures on chip [78]. Here, different concentrations of the commonly used cryoprotectant dimethyl sulfoxide (DMSO) were prepared on EWOD and its effect on cell viability was measured on chip, both before cryopreservation and after to evaluate toxicity effects of DMSO and optimal concentrations of DMSO for cryopreservation.

1.2.2 3D Cell Culture Using EWOD DMF

Section 1.1.2 identified some challenges faced by using channel-based microfluidics when attempting 3D cell culture. The challenges posed by 3D cell culture to microfluidic device adoption are more readily solved through the use of EWOD DMF. Since EWOD DMF functions in an unconstrained space without channels, there is no

chance of clogging of fluidic pathways. Also, hydrogels that are created on EWOD DMF will retain their structural integrity and will not be affected by the harsher pressure gradients that exist in continuous microfluidic devices. In addition to this, the multiplexing capabilities of EWOD make it an attractive candidate for specific applications related to 3D cell culture, such as pharmaceutical drug development, where intensive lab based experiments are carried out on potential drug candidates to screen out failure drugs based on their effects on the 3D cell culture. Since the hydrogels are encapsulated by drops, every cell seeded hydrogel is fluidically isolated from all the other hydrogels. This greater degree of isolation ensures that there is no chance of interference of drug species across neighboring 3D cell culture sites, resulting in better controlled experiments. By being able to make custom drug concentrations and deliver them to targeted culture zones, a EWOD DMF 3D cell culture chip presents itself as a versatile platform that can be used for different kinds of drug screening applications.

A conceptual EWOD DMF cell culture chip is depicted in Figure 1-6, which shows how an array of cell seeded hydrogel posts or tissue posts can be created on chip. Various liquids such as culture media (to sustain the cells), test chemicals (such as potential drug candidates), and fluorescent dyes (in order to stain cells to illuminate the effect of chemicals on the cells) can be extracted from parent reservoirs and delivered to the tissue posts on demand through EWOD actuation.

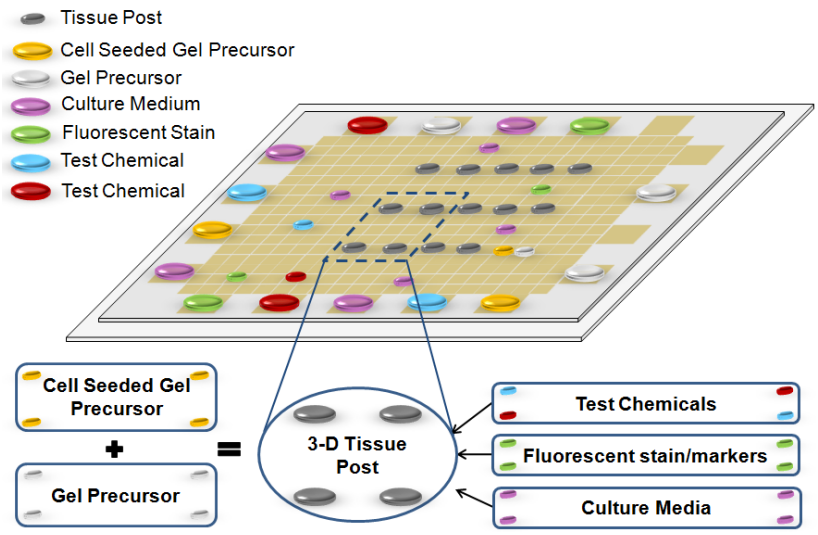

Figure 1-6 Schematic of EWOD DMF based 3D tissue based high throughput drug screening platform. 3D tissue array formation, multiplexing of chemical preparation and efficacy measurement will be done on a platform.

The initial results and findings of this research were presented in conference proceedings [79,80] and was the first to introduce the concept of 3D cell culture and chemical screening. Since then, further research has been carried out by others in the area of EWOD DMF based 3D cell culture. Fiddes et al [81] formed cell seeded agarose hydrogel discs manually off chip and then assembled them on EWOD DMF. Here, DMF was used solely as a fluid delivery platform to deliver culture media and reagents to hydrogel discs. Eydelnant et al [82] used collagen and Geltrex to demonstrate how microgels could be formed on demand on EWOD DMF and used for 3D cell culture. Au et al [83] formed hepatic organoids on EWOD DMF using collagen which was then used as a means to test toxicity of chemicals. The budding research in this field clearly indicates the novelty and impact of this research area and this thesis investigates in detail the feasibility of developing a 3D cell culture and chemical screening platform using EWOD DMF.

Chapter 2

Electro-Wetting on Dielectric (EWOD)

2.1 EWOD Theory

Electro-wetting refers to the change in contact angle that takes place when a potential difference is applied between a solid and electrolyte. This occurs because the applied electric potential causes a redistribution of charges and dipoles on the surface. The subsequent repulsion between like charges decreases the work done in expanding the surface area, which consequently results in a lowering of the interfacial surface tension as evidenced by a decrease in contact angle.

Lippmann's equation (as seen in Eq. 1), which describes the relationship between the applied electric potential (V) and the resulting surface tension (γ), can be derived through a thermodynamic analysis of the interface.

$$\gamma = \gamma_0 - \frac{1}{2} c V^2 \qquad (1)$$

where γ_0 is the surface tension of the solid liquid interface at the potential zero charge, and *c* is the capacitance per unit area.

By applying an electric field at a polarizable metal-electrolyte interface, an electric double layer (EDL) can be induced, across which a contact angle change can be observed due to the electrowetting effect. However, this contact angle change is very small and is limited by the voltage drop that can be sustained across the interface before electrolysis occurs in the liquid. Also, this contact angle change is limited to polarizable interfaces. The use of a dielectric layer between the electrode and liquid has been shown to emulate the EDL observed in conventional electrowetting, thereby allowing almost any kind of liquid to be used instead of only polarizable liquid-surface interfaces. The use of dielectrics has the added advantage of allowing much larger voltages to be applied without electrolytic breakdown of the liquid occurring, so that larger contact angle

changes can be observed. This contact angle change can be amplified further by the use of hydrophobic surface coatings. This electrowetting phenomenon that occurs through the use of dielectrics (as seen in Figure 2-1) has been termed electro-wetting on dielectric (EWOD).

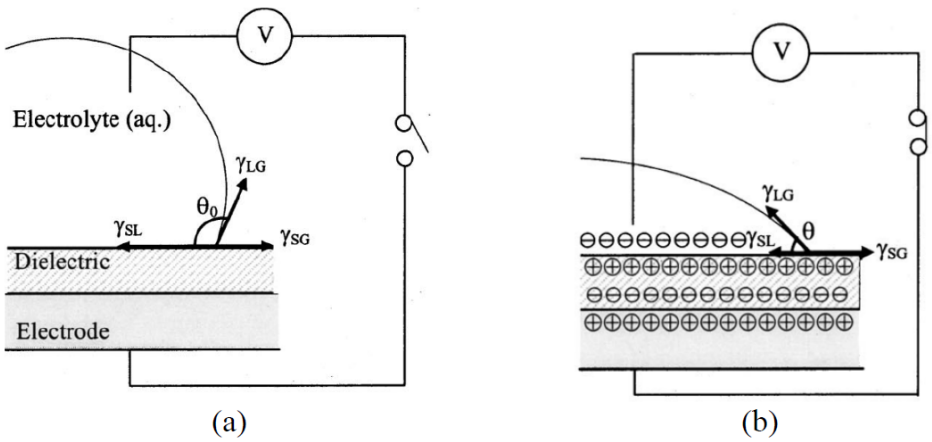

Figure 2-1 Principle of EWOD: Little or no charge accumulation occurs at the surface when no external voltage is applied as seen in (a). In the presence of an applied external voltage as seen in (b), charge accumulates at the interfaces, γ_{SL} and the contact angle θ decreases. Image taken from [46]

Young's equation provides a relationship for the contact angle of a liquid droplet on a solid surface, with surface tension, as seen below in Eq. 2

$$\gamma_{SL} = \gamma_{SG} - \gamma_{LG} \cos\theta \qquad (2)$$

where θ_0 is the contact angle when the electric field across the interfacial layer is zero, γ_{SL} is the solid-liquid surface tension, γ_{LG} is the liquid-gas surface tension, and γ_{SG} is the solid-gas surface tension.

By combining Equations 1 and 2, the Lippmann-Young equation, as seen in Equation 3 below, has been describe the contact angle changes brought about by EWOD.

$$\cos\theta = \cos\theta_0 + \frac{1}{\gamma_{LG}}\frac{1}{2}cV^2 \quad (3)$$

When a liquid drop is sandwiched between two hydrophobic surfaces, the drop will be in an equilibrium state through the balance of pressure inside and outside the drop. If the bottom layer of the sandwiched drop is now replaced by two discrete electrodes coated with a dielectric which are actuated alternatively, a contact angle change occurs due to the EWOD effect. This contact angle change disturbs the equilibrium of the drop and causes the drop to move towards the actuated electrode in order to regain equilibrium, as seen in Figure 2-2

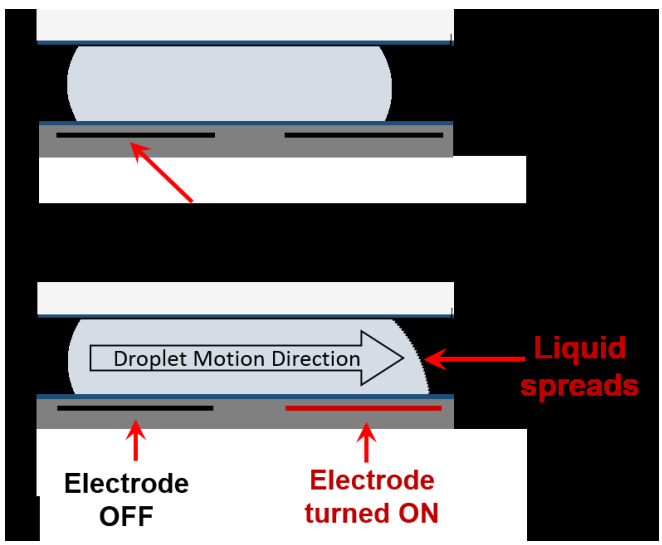

Figure 2-2 Application of EWOD to bring about liquid motion. The liquid boundary spreads over the activated electrode due to electrowetting effect.

Thus, by using an array of individually addressable electrodes coated with a suitable dielectric as a base plate and a grounded cover plate, a digital microfluidic device (DMF) can be created through sandwiched droplets can be controlled and transported simply by turning the electrodes on/off as shown below in Figure 2-3

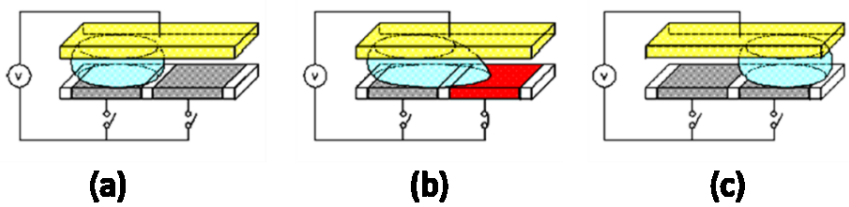

Figure 2-3 Droplet translation obtained through EWOD actuation seen in 3 stages: Droplet at equilibrium is depicted as lying over an electrode (a), but when the adjacent electrode is activated as seen by the red electrode in (b), the droplet starts to wet the activated electrode and eventually translates to it as seen in (c).

By actuating appropriate electrodes in the right sequence, basic fluid manipulation such as splitting of droplets from parent reservoirs, transportation of droplets, splitting of individual droplets, and merging and mixing of droplets can be carried out as shown in Figure 2-4. The ability to perform these operations is important since they allow EWOD DMF to be used in a variety of applications beyond just fluid transport.

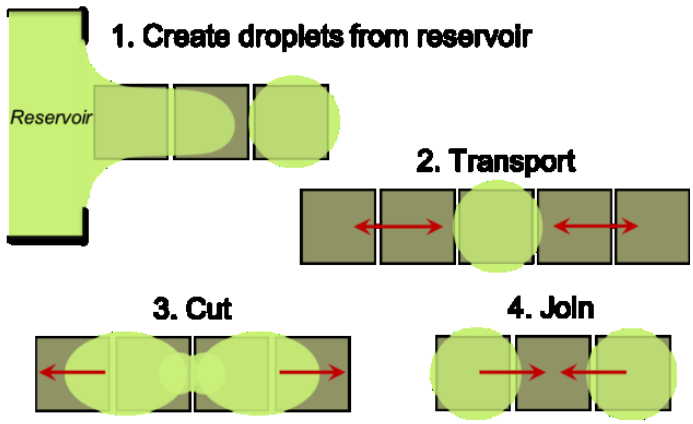

Figure 2-4 Basic fluid manipulations through EWOD actuation: 1. Droplets can be created from a parent reservoir 2. Droplets can be transported through EWOD actuation 3. A large droplet can be cut into two droplets. 4. Individual droplets can be joined to form a single droplet. Image adapted from [49].

2.2 EWOD Device Fabrication

The EWOD DMF device is composed of a bottom plate and a cover plate as shown in Figure 2-5. To fabricate the bottom plate, the first step is to pattern ITO on a glass wafer by photolithography and etching. The process to do so is as follows. First, an ITO coated glass wafer was cleaned using acetone, methanol and de-ionized (DI) water. After dehydrating by baking at 150°C for 5 minutes, an adhesive layer of hexamethyldisilazane (HMDS) was spin coated on the ITO glass wafer at 3000 rpm for 30 seconds, followed by baking at 150°C for 90 seconds. Positive photoresist Shipley S1813 was then spin coated at 400 rpm for 30 seconds followed by a pre-exposure bake at 115°C for 1 minute. The substrate was then exposed through a photomask using the OAI Backside Aligner for 7 seconds, followed by post baking at 110°C for 1 minute. Developing was done for 45 seconds using MF319 and then the sample was hard baked at 150 °C for 5 minutes. After the photolithography process, ITO etching was carried out by immersing the substrate in ITO etchant (20 wt % HCl, 5 wt % HNO3, 75 wt % H2O, or 8:1:15 vol % HCl/HNO3/H2O) at 55°C for 165 seconds. A 5 μm layer of Su8-5 was used as the di-electric layer. This was deposited on the patterned ITO wafer by spin coating at 3000 rpm for 30 seconds followed by prebaking at 95°C for 3 minutes, and then exposing to UV for 7 seconds using the aligner without a mask. Hard baking of the Su8 was done at 175°C for 10 minutes. The hydrophobic surface was created over the dielectric layer by spin coating a 2% wt/vol solution of Teflon-AF at 1000 rpm for 30 seconds followed by baking at 150°C for 10 minutes.

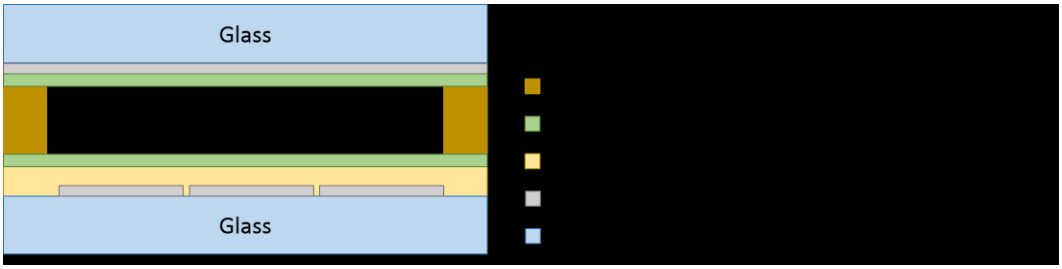

Figure 2-5 EWOD fabrication – schematic showing the composition of the the assembled device. Note that figures are not drawn to scale.

The top cover plate is prepared by first dicing an ITO coated glass wafer size, and then cleaning with acetone, methanol and DI water, followed by dehydration at 150°C for 10 minutes. Then, a hydrophobic layer of Teflon-AF is deposited and baked on in the manner described earlier for the bottom cover plate.

The device is assembled together by means of a 100 μm double sided kapton tape which serves to act as a spacer separating the top and bottom plates. Before assembly, the reservoirs are filled with appropriate liquids.

2.3 EWOD Experimental Setup and Operation

The EWOD device receives inputs through ITO based contact pads at the periphery of the device. In order to selectively address and actuate electrodes, a reliable method through which electrical signals from the control board can be delivered to the ITO contact pads is required. For the current application, a permanent connection is not desirable since the EWOD device needs to be placed in an incubator to maintain cell viability, when it is not being actively used. Thus, in order to operate the EWOD device in an automated fashion, a custom holder as seen in Figure 2-6 was designed and created which allowed for electrical signals to be delivered to the EWOD device. It consists of a base Plexiglas plate which serves to support the EWOD device and hold it in a fixed orientation, on top of which the EWOD chip is placed. Z-directional connector strips are

inserted into a specially made Plexiglas holder which is then mounted on top of the EWOD device and aligned with the base plate. A specially designed PCB board is then mounted on top of the spacers and the whole assembly is locked into place by means of screws and wing-nuts. The PCB connector board receives the signals from the EWOD control board, and then transmits it to the ITO contact pads on the base EWOD plate through the z-directional spacer.

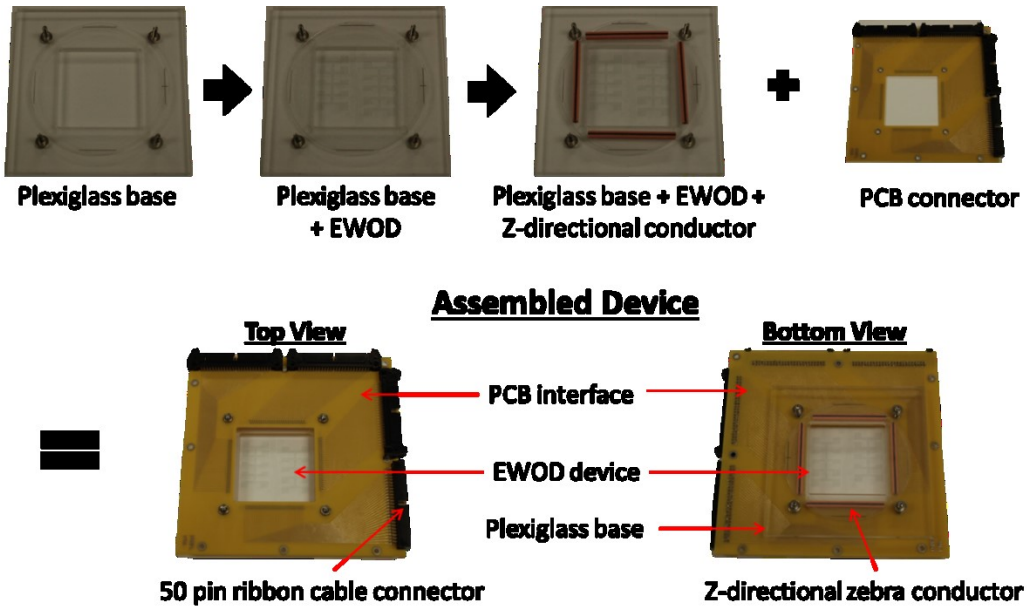

Figure 2-6 Assembly of EWOD device into automation holder: EWOD device is placed on a Plexiglas base and z-directional conductors are placed on it. A custom PCB connector board is placed on top of the conductors and locked into place to get the assembled device.

In order to operate the EWOD DMF device, a customized Control Board was used, which could transmit the EWOD driving voltages to individual electrodes of the assembled EWOD device. The EWOD driving voltages were obtained from a signal generator whose output was fed through a voltage amplifier so that an AC voltage signal

of 80-100 V and 1-10 Khz could be generated. The control board receives inputs from a Data Acquisition unit (DAQ) which in turn was controlled by a custom Labview program. The Labview program allows for electrodes to be activated, either in real time through a graphical user interface, or by feeding in sequences of operations such as drop splitting and transportation so that a completely automated process could be carried out without requiring any real time user interaction.

A digital microscope is used to observe the drop manipulations on the EWOD chip. The entire experimental setup with all the components described above, is shown below in Figure 2-7.

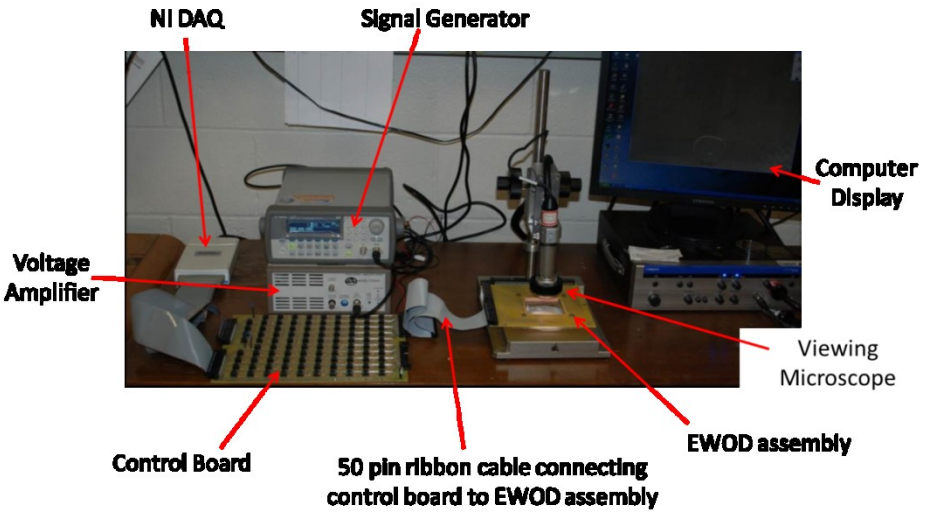

Figure 2-7 Experimental setup showing overview of the entire experimental setup.

Chapter 3

Hydrogel Formation and Characterization on EWOD

3.1 Hydrogel Selection for EWOD 3D Cell Culture

Natural extra cellular matrix (ECM) is a fully hydrated gel. Hence, naturally and synthetically derived hydrogels have been extensively used by researchers to try and mimic the ECM surrounding cells while trying to carry out 3D cell culture [84]. With regards to EWOD based approaches, hydrogels present themselves as a more conducive method to provide a 3D scaffold since they are formed by the gelation of liquid monomers.

Depending on the type of hydrogels used, the method of gelation can vary [85]. For example, hydrogels like collagen or Matrigel are naturally derived thermosetting hydrogels which are liquids that transition to gels when the temperature rises above 4˚C. PEG which is a commonly used synthetic hydrogel on the other hand can be coaxed to form a hydrogel by exposure to UV light. Both of these types of hydrogels though require additional considerations and components (such as temperature regulation devices or UV emitters) to be included along with the EWOD setup in order to be able to control gel formation at desired locations. Alginate hydrogels are a naturally derived hydrogel that are formed by adding divalent cations (such as Ca^{2+}, Ba^{2+}) to soluble sodium alginate, which results in ionic cross linkers. Since the mechanism of gelation is purely through the chemical reaction of sodium alginate with a divalent cation contributor such as calcium chloride, it is best suited for initial testing on EWOD for the feasibility of gel formation and cell viability studies.

The simple gelation mechanism of alginate, wherein a stable hydrogel can be formed at a desired location simply by the chemical reaction of sodium alginate with calcium chloride, make it ideal for use in a EWOD approach to 3D cell culturing. Other

hydrogels can also be incorporated into a EWOD device, but would require additional components such as temperature regulation devices or careful control of UV exposure in order for gelation.

3.2 Calcium Alginate Hydrogels

Calcium alginate hydrogels are commonly formed by the ionic cross-linking of sodium alginate with Ca^{2+} ions [86]. Since gelation is very gentle as well as reversible, it has found numerous applications for cell trapping and immobilization [87–89]. Calcium alginate hydrogels have also been widely documented for use in 3D cell culturing and tissue engineering [90,91]. At the macroscale, alginate hydrogels have usually been formed by dropping sodium alginate into calcium chloride baths. This has been adapted at the microfluidic scale by using channel based droplet microfluidics to generate microscale droplets of sodium alginate that are then delivered into calcium chloride solutions wherein they form calcium alginate hydrogel drops or beads [92–94]. These beads are then collected and processed separately either using other microfluidic devices or by manual handling of the alginate gel beads. Others have used continuous microfluidic devices to create cell seeded alginate hydrogels by combining laminar flows of sodium alginate and calcium chloride to examine the cell response to chemical gradients [95,96]. Still another approach that was demonstrated used spotters to create a micro-array of alginate gel spots but this approach could not address each gel spot individually and all gel spots were subject to same conditions [97].

In all the microfluidic approaches mentioned above however, alginate gelation has always been carried out either by immersing alginate drops in an abundance of calcium chloride resulting in spherical alginate beads, or by the steady continuous flow of calcium chloride over sodium alginate resulting in gel slabs. Such methods always

involve a significantly larger volume of calcium chloride being supplied to small volumes of alginate. This is however not possible in the EWOD DMF scenario since no continuous flow exists and only droplets of calcium chloride and sodium alginate are available. Despite an exhaustive literature search, no studies were found which dealt with the gelation of calcium alginate by using droplets of calcium chloride to initiate cross linking. Since this is the only means possible on EWOD DMF, this requires a study of alginate gel formation on EWOD DMF which is outlined in the rest of this chapter.

3.3 Initial EWOD Design for Gel Formation Investigation

The layout of the 1st generation design of the EWOD device that was used to test gel formation is shown below in

Figure 3-1. The design could enable up to 4 separate tissue posts to be created, and had 5 separate reservoirs to supply the tissue posts. 2 of these reservoirs were earmarked for calcium chloride and cell-seeded sodium alginate solutions which are required to form the calcium alginate gel. This left 3 remaining reservoirs that could be used for any other reagents/media such as culture media or fluorescent dyes. The smallest electrodes were 2mm x 2 mm squares and when combined with a 100 μm spacer gap, allowed for drops of 400 nanoliters to be discretized.

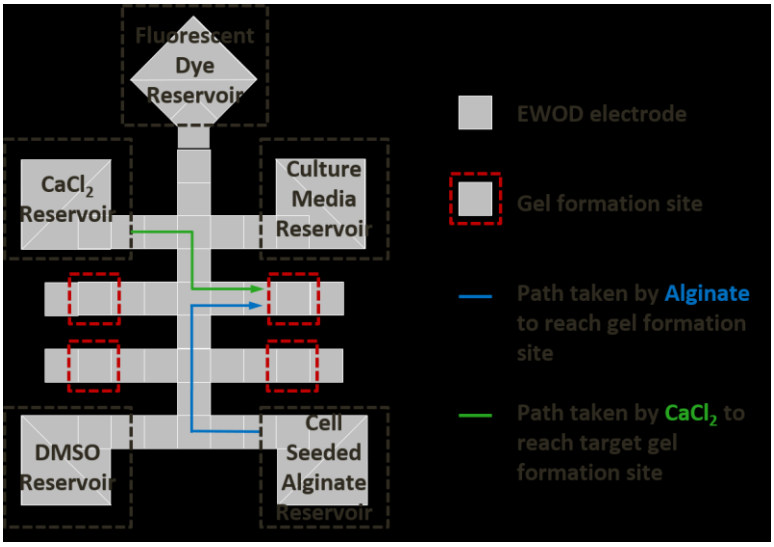

Figure 3-1 Layout of 1st generation EWOD device used for tissue post creation and screening. The blue and green arrows depict the path taken by cell seeded Sodium Alginate and Calcium Chloride to reach one target post site from their respective reservoirs.

3.4 Materials and Methods

3.4.1 Cell Culture

NIH 3T3 fibroblast cells (MCF-7) were maintained in culture medium (D-MEM, Life Technologies, Carlsbad, CA), and supplemented with 10% fetal bovine serum, 2 mM l-glutamine, and 100 µg/mL penicillin/streptomycin. Cells were incubated in 75 cm^2 T-flasks at 37°C and 5% CO2 while being sub-cultured every 3-4 days at ~ 80% confluence.

3.4.2 Gel Precursors

Low viscosity sodium alginate powder (Sigma Aldrich, St. Louis, MO – CAS 9005-38-3) was dissolved in deionized water to obtain 0.5%, 1% and 2% wt/vol concentrations of sodium alginate solutions.

To prepare cell seeded sodium alginate solutions, 3T3 cells that had reached 80% confluence in T-75 flasks were trypsinized and centrifuged. The resulting cell pellet was resuspended in 0.5%, 1% and 2% sodium alginate solutions to obtain cell seeded sodium alginate solutions with a cell density ~ 1 x 10^6 cells/mL.

100 mM calcium chloride solutions were prepared by dissolving calcium chloride crystals (Sigma Aldrich) in deionized water.

3.4.3 Device Fabrication and Operation

EWOD devices were fabricated and operated in the manner previously described in sections 2.2 and 2.3 using the mask described earlier in section 3-2.

0.3 µl volumes of cell seeded sodium alginate solutions and calcium chloride solutions were placed in parent reservoirs of the bottom EWOD chip before placing the top cover slip over the bottom chip.

For device operation, A.C sinusoidal voltages ranging from $55V_{rms}$ to $150V_{rms}$ were applied at 1 KHz frequency using the signal generator and voltage amplifier to actuate the electrodes for EWOD drop motion.

3.4.4 Gel Formation Protocol

The basic protocol of gel formation on EWOD DMF consisted of first extracting a drop of cell seeded sodium alginate from its parent reservoir as shown below in Figure 3-2 (a)-(c). In a similar manner, an equal volume of calcium chloride is extracted from its parent reservoir. The sodium alginate and calcium chloride drops are transported to the gel formation site by EWOD actuation and allowed to merge in a 1:1 ratio at the gel formation site as shown in Figure 3-2 (d). After allowing sufficient time for gelation,

excess liquid formed as a byproduct of gelation would be removed (see Figure 3-2 (e)) from the gel and transported to the waste reservoir.

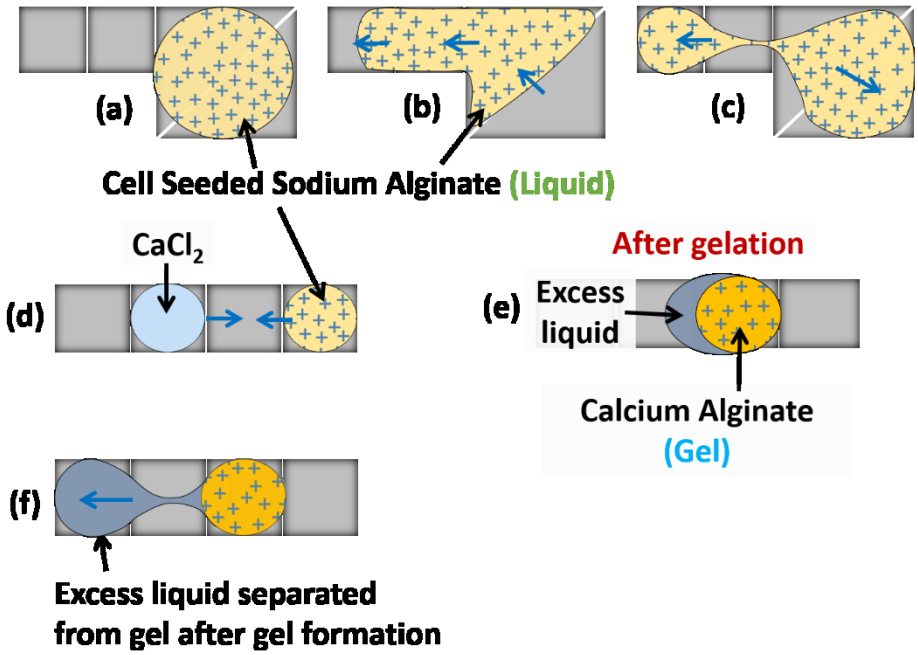

Figure 3-2 Schematic of gelation protocol in EWOD DMF: (a)-(c) Cell seeded sodium alginate solution droplet generation from the reservoir, (d)-(e) formation of calcium alginate gel post, and (f) extraction of excess liquid. Blue arrows indicate direction of drop motion by EWOD electrode actuation.

3.5 Results and Discussion

3.5.1 Determination of Sodium Alginate Concentration for Motion on EWOD

Before alginate gels could be made, it is important to first determine the concentrations of sodium alginate that can be moved on the EWOD platform. The viscosity of sodium alginate increases as its concentration increases. This can be challenging for EWOD applications since liquids of high viscosity tend to move slowly on chip and are also difficult or impossible to split into smaller drops on chip.

Initial testing of sodium alginate compatibility with EWOD actuation was attempted by using concentrations of 0.5%, 1% and 2% w/v ratio solutions of sodium alginate. 0.3 µl drops of all three solutions were placed in separate reservoirs and drops were split from parent reservoirs. Split drops were transported on chip and the voltage required for successful drop splitting and motion was noted.

The 2% sodium alginate solution was the most viscous solution attempted and splitting drops from the parent reservoir proved to be impossible even at high voltages since no neck could be formed during the drop splitting process. However, the parent drop itself was responsive to EWOD actuation and could be transported as a large drop. This was not practical for the purpose of forming discrete gels on chip and so 2% alginate solutions were not considered.

1% sodium alginate solutions were less viscous than the 2% solution and drops could be split and transported on the chip at higher voltages (~150V). However, at more reasonable voltages (~80-90V), drop motion was very slow and drop splitting could not be achieved.

The 0.5% sodium alginate solution was the least viscous of the alginates tested. Drops could easily be split and transported from the parent reservoir at normal operating voltages (~80-90V). However, it was observed that when compared to water, longer necks were formed during drop splitting and this resulted in dispensed drops that were of larger volumes than comparable drops formed from plain water.

Of the 3 sodium alginate solutions tested, 0.5% wt/vol alginate solutions proved to be the most suitable for EWOD operation and was selected as the default concentration for all further experiments.

3.5.2 Gel Formation Confirmation

Drops of 0.5% cell seeded sodium alginate solution were split at ~80-90V_{rms} from the parent reservoir and transported to the gel formation site. Following this, drops of 0.1 M $CaCl_2$ solution were split and brought to the gel formation site where they were allowed to merge with the sodium alginate drop.

After merging the sodium alginate and calcium chloride drops and allowing 15 minutes for gelation, a clear interface could be seen consisting of an outer clear phase and an inner cell-containing phase. The outer phase behaved as a liquid and responded well to electrode actuation. The inner cell-containing phase was unresponsive to electrode actuation though it could be dragged by the outer liquid phase when the outer liquid phase was moving. Even though the inner phase could be moved by the outer liquid phase, the cells within the inner phase remained fixed in place relative to other cells. This is in contrast to cells in the cell seeded liquid sodium alginate drops prior to merging, which would recirculate within the sodium alginate drop during sodium alginate drop motion. Thus the lack of cell motion relative to other cells in the inner phase confirmed that this inner phase was behaving more like a solid than a liquid. This led to the conclusion that the inner phase was the calcium alginate hydrogel that had immobilized the cells and the outer phase was the excess liquid formed after gelation.

The experimental results showing how gel precursors are delivered to the target site and gel formation occurs are depicted in Figure 3-3, along with a magnified view of the cell seeded calcium alginate hydrogel where a clear boundary can be seen separating the gel from the surrounding liquid.

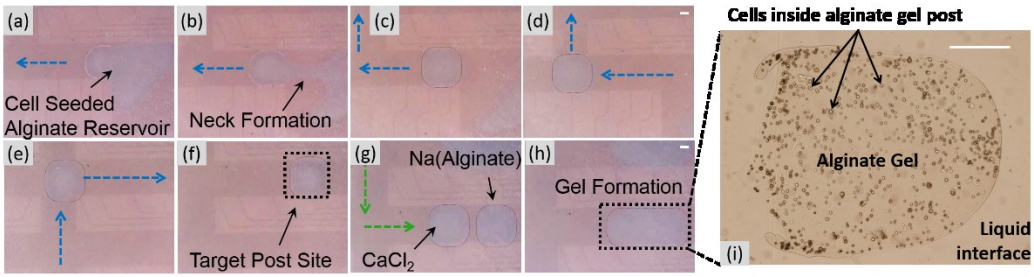

Figure 3-3 Cell seeded alginate drop (A) is separated from reservoir (a)-(c) followed by transportation towards destination site (d)-(f). $CaCl_2$ (B) is brought to cell-seeded alginate (g) which results in gel formation (h), seen in greater detail in (i). Thus gel formation capability is demonstrated on EWOD chip. Blue and green arrows represent sodium alginate and $CaCl_2$ flow pathways respectively. Scale bar represents 500 µm

3.5.3 Excess Liquid Removal From Gel and Factors Affecting It

Once the calcium alginate gel has been formed, the next step is to remove the excess liquid by products of gelation. Excess liquid removal of excess or waste liquid from a gel post is an essential step before new liquids are delivered. Otherwise, cell metabolism waste products would accumulate and lead to toxic conditions affecting viability. If liquid delivery to the gel post is continued without waste liquid removal, then liquid accumulation would occur. Large pools would eventually form around the gel rendering it ineffective from a chemical screening point of view since any chemicals delivered would be diluted to unknown concentrations.

When excess liquid removal was attempted by actuating the electrodes adjacent to the gel drop surrounded by excess liquid, either the gel moved along with the liquid, or the gel itself obstructed the flow of liquid. In either scenario, excess liquid separation was not possible.

Repeated experiments were carried out to identify the factors that were responsible for preventing consistent excess liquid removal and are discussed below:

3.5.3.1 Gel size

The current alginate gels that were formed were of the same dimension as that of the electrode dimension. This resulted in the gel itself being an obstruction to the flow of liquid around it and made it difficult for excess liquid to be removed. To counter this, either extra electrode pathways would have to be provided around the gel formation site, or the size of the gel itself would have to be reduced.

Adding extra electrode pathways around the gel formation site for excess liquid removal however would not be optimal. The addition of extra electrode pathways around each gel formation site would increase the gel-to-gel distance and thus prevent gel formation sites from being closely packed together. While this might not be a problem for small number of arrays, it would result in devices that have a very large footprint when designing devices that need to form a larger array of devices. Also, adding extra electrode pathways would complicate the DMF design since routing more electrode connections in a finite 2D space would be difficult.

The more easily adoptable approach is to reduce the gel size. Having a gel that is smaller than the electrode pathways would ensure that liquid flows around the gel to reach the adjacent electrode. The difference between gel sizes of comparable dimension to electrode dimension and smaller gels is schematically shown in Figure 3-4. Also, smaller gel sizes relative to other liquid drops would mean that culture media being supplied to the gel would be much larger relative to the gel size. This would help to ensure that culture media replenishment could be stretched out and not have to be done as frequently as in the case where gel size is equal to culture media volume.

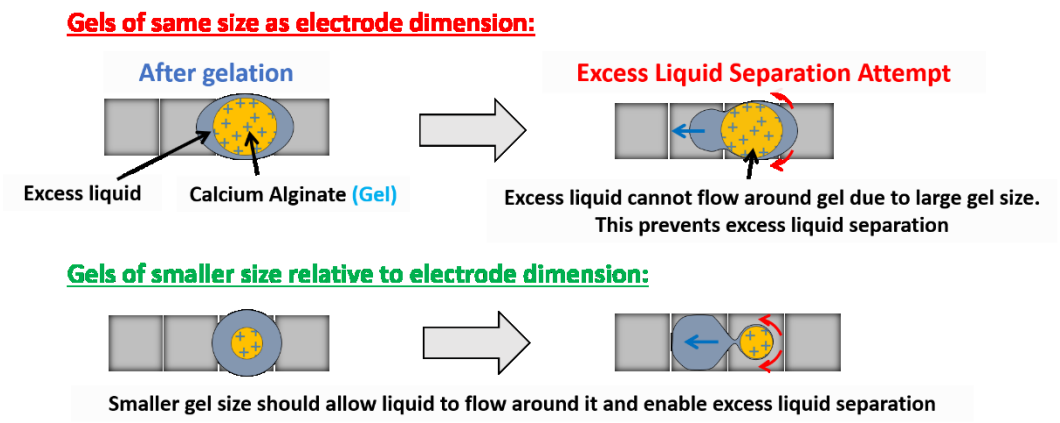

Figure 3-4 Gel sizes of same size as electrode dimensions obstruct flow of liquid around gel preventing excess liquid separation. Smaller gels could eliminate this problem.

3.5.3.2 Gel anchoring

Anchoring of the gel was determined to be a major issue that greatly affected the ability to separate excess liquid from the gel post. During excess liquid removal attempts, situations arose where the gel itself got carried away with the excess liquid, making excess liquid removal impossible.

While the gel itself behaves like a solid and does not respond to EWOD actuation, the liquid surrounding it was found to be able to move the gel along with it during excess liquid removal. In the few cases where the gel was anchored, excess liquid separation was achieved. However, in all the remaining cases, the gel either “floated” away with the excess liquid, or got “dragged” by it. The difference caused by sufficient anchoring as opposed to insufficient anchoring on excess liquid separation is schematically shown in Figure 3-5.

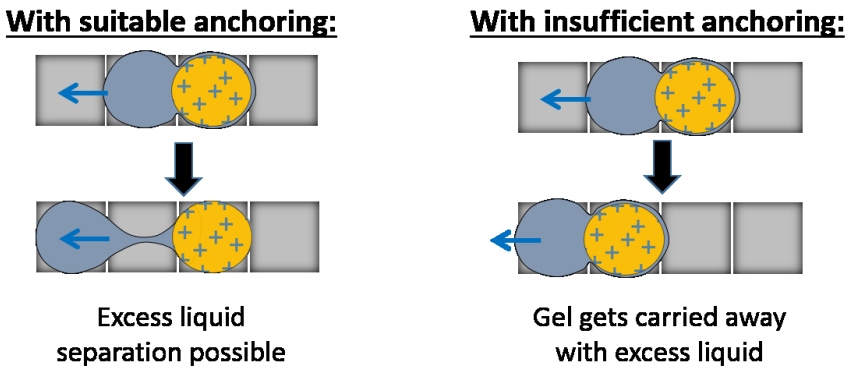

Figure 3-5 Excess liquid separation possible when gel is suitably anchored. However, when anchoring is insufficient, the gel gets carried away with excess liquid.

In cases where the gel was “floating”, the gel was always surrounded by liquid and got carried away in the middle of the drop. It is theorized that in the floating scenario, a thin liquid film layer exists below the gel and acts as a lubricant allowing the gel to move easily along with the bulk liquid. Such floating gels offered minimal resistance to fluid flow and easily got transported away with the excess liquid all the way to the waste reservoir. During attempts to remove excess liquid from such gels by applying forward and backing force on the gel-drop system, the gel always got caught in the middle and prevented neck formation. Neck formation is a vital prerequisite for drop splitting and separation on EWOD DMF and without the formation of a neck, applying forward and backing forces on the drop just result in a tug of war with the whole drop moving to whichever side can generate the greater force.

In cases where the gel was “dragged”, it was clear that the gel itself was providing resistance to fluid flow. This was apparent by the way the gel moved with the liquid – the gel always occupied the rear portion of the drop with the excess liquid always rushing to fill the adjacent actuated drop and dragging the gel along with it. Quick actuation of a series of adjacent electrodes could separate the excess liquid from the gel,

since there was a clear difference in response of liquid and gel to EWOD actuation. However, this still left the gel displaced from its original gel formation location and in the middle of regular fluid flow paths where it would get in the way of other reagents like culture media, fluorescent dyes or test chemicals and contaminate them.

Thus, regardless of whether the gel “floated away” or got “dragged” by the excess liquid, it was clear that without a means to hold the gel fixed in place, attempts at excess liquid separation would not succeed since the gel would get transported away with the excess liquid instead of being separated from it. Having a means to hold the gel in place and anchored is thus a vital requirement for successful excess liquid removal.

3.5.3.3 Gel shape

Perhaps the biggest factor affecting excess liquid removal from the gel is the shape of the gel. Irregular gel shapes resulted in the irregular boundaries which impacted the way fluid flows around the gel. The greater the irregularity of the gel shape, the greater resistance it provides to fluid flow around it. In some cases, the gel boundaries were such that pockets were formed which trapped liquid behind it, making it impossible to effectively remove excess liquid from the gel as shown in Figure 3-6. Having a smooth gel shape that allows fluid to flow freely around it can help prevent the gel from trapping liquid and being pulled away with the excess liquid. The factors affecting gel shape are discussed in more detail in the following section.

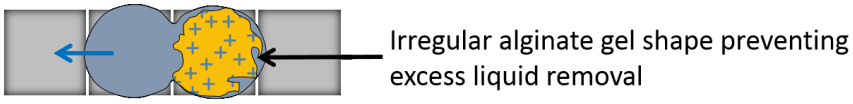

Figure 3-6 Irregular gel shapes create resistance to fluid flow and prevent excess liquid removal.

3.5.4 Importance of Gel Shape and Factors Influencing Gel Shape

The shape of the gel affect the ease with which excess liquid can be separated as discussed earlier. However, even in cases where excess liquid separation is possible due to robust anchoring, the shape of the gel can still pose problems for use as a 3D cell culturing and chemical screening platform. The pockets of liquid trapped by irregular gel boundaries can dilute any incoming chemicals. This would create a variable chemical concentration gradient around the gel itself and can hinder the accurate evaluation of chemical concentration and gradient effects on cell response. This would create additional variables in experiments that could not be reliably accounted for and result in flawed data. The following factors were found to influence the shape of the alginate gels formed:

3.5.4.1 Method of Delivery

It was observed that the method of merging the sodium alginate and calcium chloride drops affected the shape of the resulting gel. Because of the rapid nature of calcium alginate gelation, any time an exposed boundary occurs

Moving sodium alginate drops to merge with stationary calcium chloride drops resulted in gels of the shape seen in Figure 3-7 (a). The moving sodium alginate drop tended to wrap itself around the stationary calcium chloride drop resulting in highly irregular gel shapes characterized by thin long tails on the forward merging side and a thick long tail at the receding side. Due to the tail formations, the gel itself would exist stretched out beyond the

When sodium alginate drops were kept stationary and calcium chloride drops were moved, the irregularity in gel shapes were less prominent as seen in Figure 3-7 (b). The gels formed were well contained within a single electrode volume.

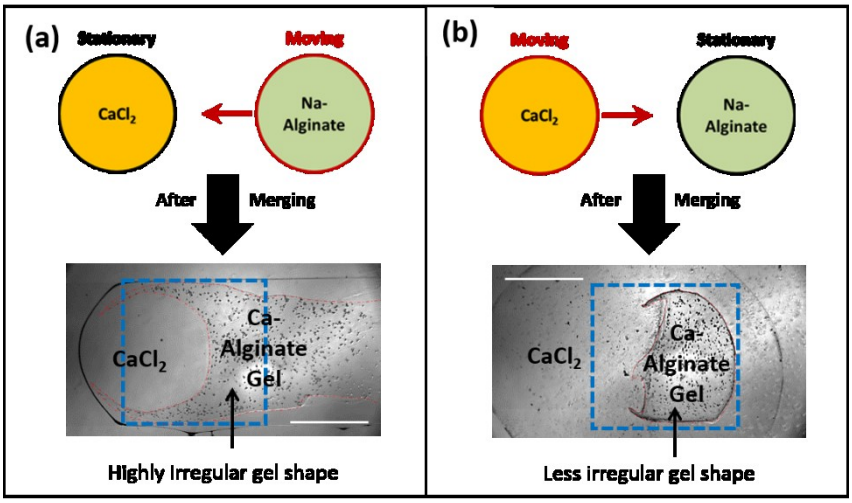

Figure 3-7 (a)-(b): Methods of merging sodium alginate and calcium chloride drops and the resulted gel shapes. Red dotted lines were added to figure to help identify the gel boundaries while blue dotted lines indicate electrode boundaries. Scale bars represent 0.5mm

3.5.4.2 Actuation before complete gelation

It was found that enough time should be provided for complete gelation. The gelation of alginate is caused by cross-linking of alginate chains by calcium ions. The degree of cross-linking is affected by the concentration of calcium ions and time allowed for gelation. Thus, an alginate that has transitioned to a gel like state can still continue to form cross-links between alginate molecules resulting in a more dense and rigid gel. In order to avoid confusion, the term “complete gelation” that is used hereafter in this work refers to the point at which the alginate has transitioned from the solution phase to the gel phase with no liquid moveable parts. Complete gelation as defined in this method has no bearing on the degree of crosslinking but only refers to the point at which a phase change from liquid to gel is observed (since crosslinking can continue to occur even after the alginate has become a gel).

When the calcium chloride drop is merged with sodium alginate, gelation at the interface is almost instantaneous, resulting in the formation of a thin hydrogel layer. If the system is disturbed through EWOD actuation before sufficient time has been provided for complete gelation (15 minutes in this case), the liquid components of the system (calcium chloride and sodium alginate) respond to EWOD actuation while the thin layers of calcium alginate hydrogel already formed remains unresponsive. Due to this relative motion of the liquid components of the partly gelled system, new interfaces between sodium alginate and calcium chloride were created resulting in instantaneous gelation at the newly exposed interfaces. This had the effect of creating irregular gel shapes as shown in Figure 3-8 where the gel system was disturbed after allowing only 5 minutes for gelation as opposed to the regular 15 minutes normally provided.

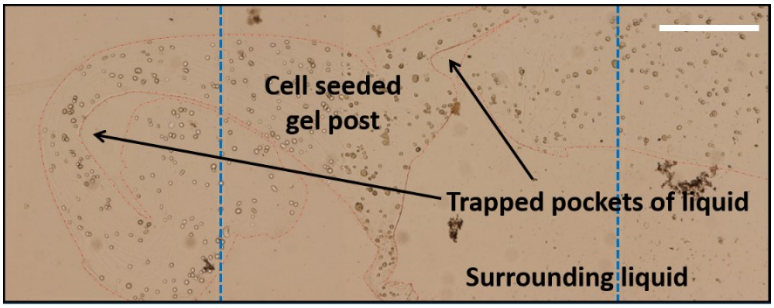

Figure 3-8 An example of irregular gel shapes when the merged sodium alginate – calcium chloride drops are actuated before complete gelation. Red dotted lines were added to figure to help identify the gel boundaries while blue dotted lines indicate electrode boundaries. Scale bar represents 0.5mm

3.6 Alginate Gelation Modeling to Determine Time for Gelation

3.6.1 Introduction

The need for size reduction of alginate hydrogels was determined in section 3.4.4. For smaller gels, the time for gel formation would obviously be lower, but to experimentally detect whether complete gelation has occurred or not is very difficult to

determine at the microscale. A theoretical model for alginate gelation would help provide some guidelines for the time required for complete gelation for different gel geometries. This is also beneficial to know in order to avoid scenarios described in section 3.5.4.2 where premature actuation of gels before complete gelation results in irregular gel shapes.

The gelation mechanism of alginate hydrogels involves a phase change transition since calcium ions (Ca^{2+}) react with sodium alginate to form a solid calcium alginate hydrogel. For gelation to continue, Ca^{2+} ions then have to diffuse through the newly formed calcium alginate hydrogel layer in order to reach the unreacted sodium alginate. Thus, until the system has reached a steady equilibrium state (wherein all the alginate ions or all the Ca^{2+} ions have been consumed), the Ca^{2+} ions have to diffuse through an ever increasing calcium alginate gel section in order to reach the sodium alginate liquid. This is what essentially constitutes a moving boundary problem where a phase change system is characterized by a moving boundary that is time dependent. Figure 3-9 depicts the gelation process of calcium alginate.

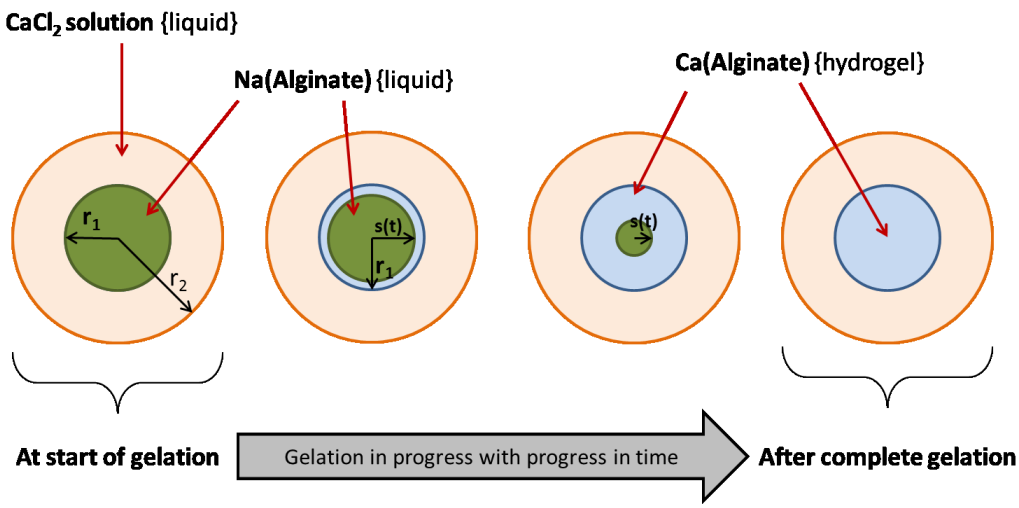

Figure 3-9 Gel formation schematic showing how the liquid system transitions into a gel, by the diffusion of Calcium ions from the outer $CaCl_2$ liquid drop to the central Na-Alginate liquid core. Gel formation occurs as calcium ions react with alginate residues and the position of the solution-gel moving boundary is described by radius s (t) which varies with time t. S(t) is initially equal to the radius of the Na-Alginate drop r1, but decreases and tends to zero as time progresses and gelation completes.

While the moving boundary problem for calcium alginate gelation would provide an exact time frame for the time required for gel formation to occur, its solution is not a trivial matter. Inoue provides a detailed analysis of the solution to the moving boundary problem for calcium alginate at the macroscale in her dissertation work [98].

3.6.2 Simplified Diffusion Model for Alginate Gelation

For the present study, only a rough estimation of time required for gelation would be required. Thus, instead of developing a microscale model using the moving boundary method, a simplified model was attempted.

Many studies have suggested that the actual reaction time for calcium ions to bind with sodium alginate is negligible. In such a scenario, the bulk of the time required for gelation would actually be limited by the diffusion of calcium ions through the already

formed calcium alginate hydrogel to reach the sodium alginate interface. This would then do away with the need to consider reaction time between sodium alginate and calcium ions.

An even larger approximation that was then made is to assume that instead of dealing with a moving boundary, the entire sodium alginate is replaced with a solid calcium alginate hydrogel. This would then lead to a simplified scenario that deals only with the 1-d diffusion of calcium ions through a calcium alginate hydrogel. This diffusion model would be able to predict the calcium concentration throughout the gel at any given moment of time. By calculating the required concentration of calcium ions to completely bind with alginate ions, and then calculating for the amount of time required for the calcium concentration in the hydrogel to reach this concentration, we could arrive at a very simplified approximation for time required for gelation.

In order to try out this simplified diffusion model, 2 different situations were considered as seen in Figure 3-10. The first scenario attempts to replicate the experimentally formed gels that were obtained on chip. This involved the merging of equal volumes of large drops of sodium alginate and calcium chloride, both of which were transported on electrodes of 2mm x 2mm size. The second scenario explores the usage of a smaller gel as recommended in section 3.4.4. Here a smaller circular gel is sought to be created with the same volume as that held by a 1mm x 1mm electrode. The radius of such a gel is ~ 0.56mm. Gel formation in this scenario would occur by delivering a larger drop of calcium chloride through a 2mm x 2mm electrode to this smaller circular gel. Since the volume of the calcium chloride is now 4 times larger than the alginate volume, it is assumed that the calcium chloride drop envelops and encapsulates the alginate drop, necessitating the use of a diffusion model in radial co-ordinates.

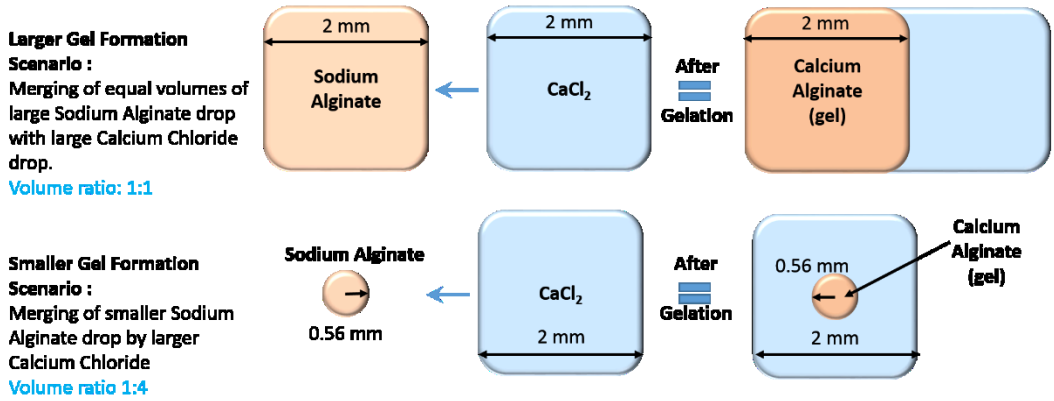

Figure 3-10 Two different scenarios proposed to be solved by simplified diffusion model. The first scenario is based on the method of gel formation that was experimentally carried out using equal volumes of sodium alginate and calcium chloride. The second model attempts to model a scenario where the gel size is reduced while the calcium chloride delivered is still the same size.

Since the simplified diffusion model reduced the gelation model to a 1D diffusion of a single species (calcium ions) through a gel of known dimension, the problem became relatively simple to solve. COMSOL was used to model and solve the diffusion of calcium ions through the above situations mentioned above. For both models, the only variations lay in the geometry which is shown in Figure 3-10 above. All other parameters remained the same in both cases.

Fick's 2nd law of diffusion was used as the governing equation in COMSOL to provide a relation between the instantaneous concentration of calcium ions (C) with variation with distance (x) and time (t). Since diffusion was being modeled in 2 regimes – calcium chloride and calcium alginate gel, separate governing equations had to be used as seen in equations (4) for diffusion in calcium alginate gel and (5) for diffusion in calcium chloride solution.

$$\frac{dC}{dt} = D_{CA}\frac{d^2C}{dx^2} \quad (4)$$

$$\frac{dC}{dt} = D_{CC}\frac{d^2C}{dx^2} \quad (5)$$

From literature [99], the diffusivities of calcium ions in a 1% wt/vol calcium alginate gel (D_{CA}) was taken as 0.8 x10^{-9} m^2/s and the diffusivity of 100mM calcium ions in calcium chloride solution (D_{CC}) was taken as 0.78x10^{-9} m^2/s.

The initial concentration of Ca^{2+} ions within the calcium alginate gel was assumed to be zero with the assumption that all the Ca^{2+} ions were bound to alginate at time t=0. The initial concentration of Ca^{2+} ions at the boundary where calcium chloride was in contact with the calcium alginate gel was taken as 100 mol/m^3 based on the usage of 100mM calcium chloride solutions in the experiment.

For boundary conditions, wherever an interface occurred between calcium chloride and calcium alginate, a constant concentration boundary condition was assumed such that the calcium concentration at the shared boundary of calcium alginate and calcium chloride was constant. In the case of the larger gel formation scenario, an insulation boundary condition was assumed for the calcium chloride and calcium alginate drops that were exposed to air since no calcium ion diffusion occurred across the liquid air boundaries. In the case of the smaller gel formation scenario, only calcium chloride had a boundary exposed to air, so an insulation boundary was assumed there. The calcium alginate gel was surrounded by calcium chloride uniformly, so for calcium alginate, a symmetry boundary condition was also assumed at the center of calcium alginate gel.

Solving the larger gel formation scenario gave the results as seen below in Figure 3-11. The graph shows the concentration profile of calcium ions in both the calcium chloride solution and the calcium alginate gel as time progresses.

Larger Gel Formation Scenario

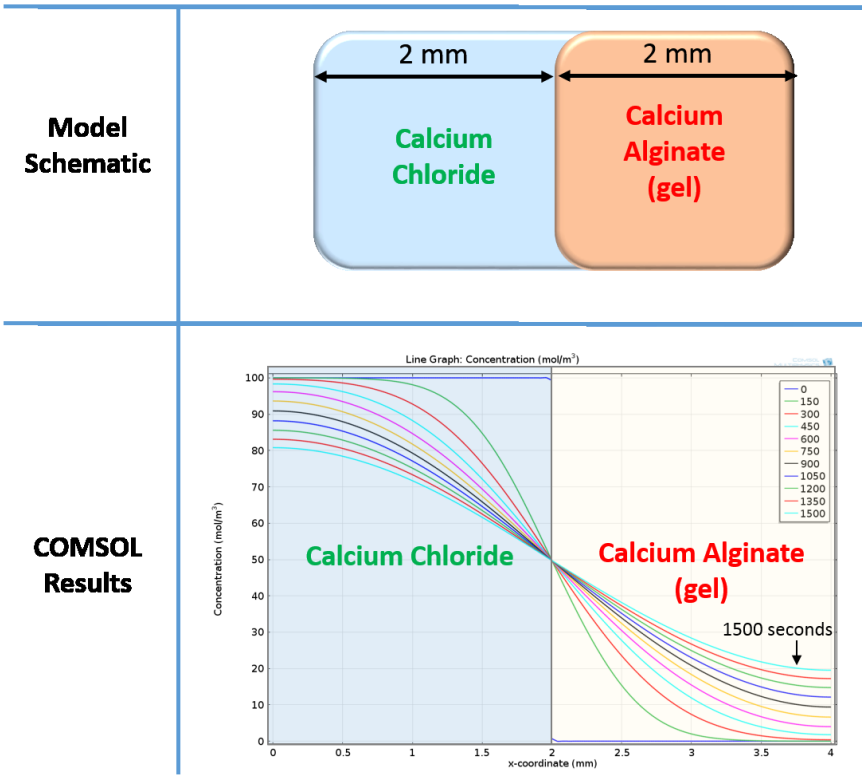

Figure 3-11 COMSOL solution of diffusion of calcium ions from calcium chloride solution through a calcium alginate gel of equal volume. The results are in the form of a concentration profile that show how calcium concentration varies in both the calcium chloride solution the calcium alginate gel over time.

Similarly, solving for the smaller gel formation scenario gave the results as seen below in Figure 3-12. The graph shows the concentration profile of calcium ions in both the calcium chloride solution and the calcium alginate gel as time progresses.

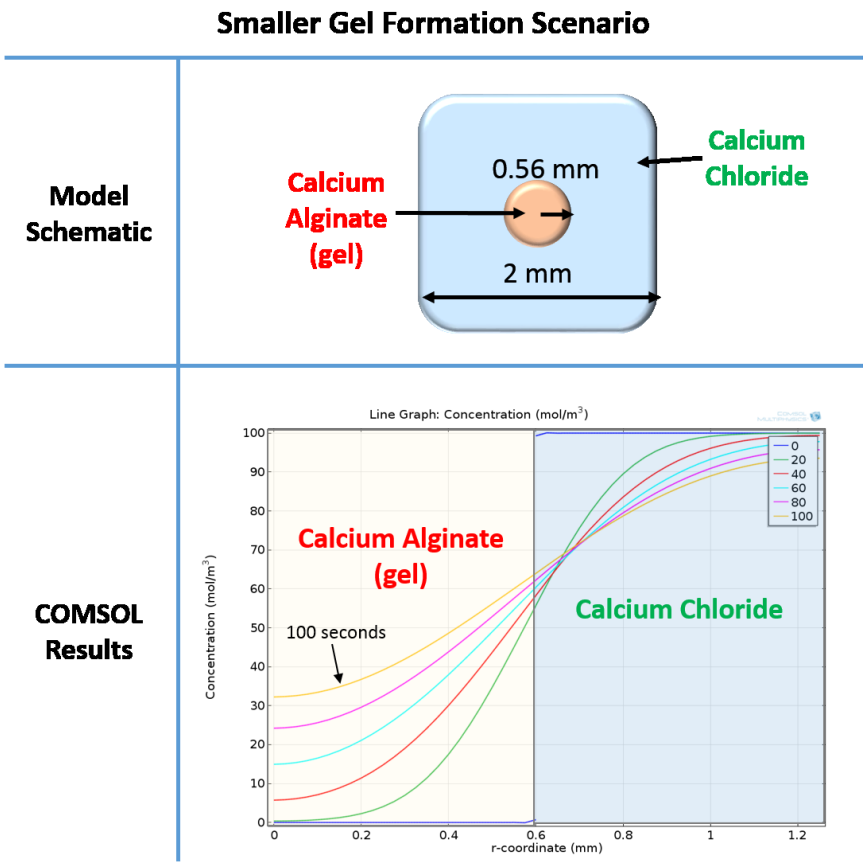

Figure 3-12 COMSOL solution of diffusion of calcium ions from calcium chloride solution to a smaller calcium alginate gel of 1/4th volume of calcium chloride drop. The results are in the form of a concentration profile that show how calcium concentration varies in both the calcium chloride solution and the calcium alginate gel over time. Note how the calcium ion concentration within the calcium alginate gel increases much faster with time when compared to the larger gel formation scenario.

When comparing closely the concentration profile results obtained for both the larger and the smaller gel formation scenario, it is evident that the calcium ion concentration rises much more rapidly in the smaller gel. Even after 1500 seconds (25 minutes), the lowest value of calcium ion concentration at the larger gel formation scenario is less than the value of calcium ion concentration in smaller gel formation

scenario after 100 seconds. Thus, clearly, the size and method of calcium chloride delivery can clearly affect the rate of diffusion on the calcium alginate hydrogels.

However, concentration profile alone does not provide a value for the time taken for gelation to occur. In order to calculate the time of gelation, we need to know the minimum threshold calcium ion concentration required to ensure that all alginate ions have free calcium ions to bind with.

In order to do this, first the alginate concentration within the existing sodium alginate drop needs to be calculated. Based on the sodium alginate manufacturer's specifications, the alginate supplied has a molecular weight ranging from 120,000-190,000 g/mol. Thus, by assuming an intermediate value of 150,000 g/mol and a 0.5% wt/vol sodium alginate solution, the molar concentration of 0.5% wt/vol alginate solution can be calculated as 0.0333 mol/m^3.

The required calcium ion concentration needed to completely bind with this 0.333 mol/m^3 concentration of alginate ions could then be calculated if the number of calcium ions that bind to alginate were known. One calcium ion can form cross-links between two alginate molecules. However, alginate molecules are long chain polysaccharides and there exists multiple binding sites on the alginate chain for the calcium ions to bind to. This makes it impossible to determine the number of binding sites for calcium ions on alginate, especially since the mechanism of calcium binding to alginate ions is still an evolving field [100,101]. Thus, determining the number of calcium ions required to bind to alginate ions for gelation to occur becomes impossible.

Therefore, another method to determine time for gelation based on the calcium concentration graphs provided by COMSOL is required. From the initial alginate gelation experiments, 15 minutes was observed to be sufficient time for complete gelation in the 1:1 direct merging method carried out on 2mm x 2mm electrodes. Comparing this with

the calcium concentration profile for the COMSOL results for the 2mm x 2mm larger gel scenario, 15 minutes (=900 seconds) corresponds to a minimum calcium concentration of ~10 mol/m^3 that occurs at the location in alginate farthest away from the merging interface. Assuming this as the threshold minimum calcium ion concentration for complete gelation to occur, the time for the smaller gel formation case to reach a minimum concentration of 10 mol/m^3 throughout the gel is determined to be ~ 50 seconds.

The diffusion model that was devised above was only meant to provide a rough approximation and the validity of the model remains yet to be proved. The model revolves around many assumptions that were made in order to simplify the calculations but such assumptions could result in incorrect time for gelation. Regardless of the accuracy of the time calculated for complete gelation, the model still does successfully show that calcium ion diffusion in the smaller gel formation model using the 1:4 encapsulation method is significantly faster than that which occurs in the larger gel formation model using 1:1 direct merging.

In an attempt to determine more feasible predictors of gelation time at the microscale, an exhaustive literature review was carried out. A recent study of calcium alginate gelation at the microfluidic scale by Braschler et al [99] was discovered wherein they used a much more complicated version of the moving boundary problem to model the gelation of calcium alginate. This model accounted for both calcium ion diffusion as well as alginate diffusion within the gelling system and also considered the reaction time involved in the binding of calcium ions with alginate ions. The results of Braschler's study shows that for the gelation of 1% wt/vol calcium alginate, length scale greatly impacts the diffusion rate. By extrapolating their predicted time for gel formation for a given distance, it was determined that for 1% alginate gelation to reach a 2mm length, the time involved

would be ~ 22 minutes. However, shrinking down the length scale to 0.6 mm would only require ~ 5 minutes.

Experimental methods for gel formation revealed that for a 0.5% alginate gel to grow 2mm, ~ 15 minutes would be required for complete gelation. This is consistent with Braschler's study since a 0.5% alginate gel will form a gel much faster than a 1% alginate gel.

3.7 Conclusion

Calcium alginate gelation was tested on EWOD DMF and factors affecting reliable gel operation were determined. The necessity for successful excess liquid removal was identified as well as the factors that affect it. The importance of controlling gel shape was also recognized in order to consistently produce gels of uniform shape. If shape variations occurred from gel to gel, then extra variables would be introduced into the experiment such as variations in surface area and local chemical concentrations. A diffusion model of alginate gelation was attempted to identify time required for gelation for various gel shapes which helped demonstrate the benefits of an encapsulation design with regards to reducing the time required for gelation.

Chapter 4

Design Optimization for Reliable Gel Formation

4.1 Introduction

In order for a EWOD DMF device to be suited for 3D cell culture applications, it is essential that consistent gels can be formed on demand as well as be reliably addressed by culture media and reagents. The previous chapter identified factors involved in the gelation of alginate that could affect both gel shape as well as the ability to remove excess liquids successfully. Both of these factors play an essential role in ensuring that gels of consistent shape can be formed and addressed by liquids. Thus, by optimizing the EWOD DMF design to accommodate and account for these factors, a reliable method for the creation and maintenance of hydrogel based 3D cell cultures is developed as outlined below.

4.2 Size Reduction and Circular Gel Formation Electrodes (Design A)

4.2.1 Objective

One of the first issues identified with the test EWOD DMF device in chapter 3 was the size of the hydrogel. Having a hydrogel of the same size as the electrode pathway dimension (2mm x 2mm) resulted in large gels that took longer to gelate and also blocked the flow pathway, making excess liquid removal difficult or impossible.

The diffusion analysis of section 3.6 demonstrated that a smaller gel would take significantly less time to form a gel. Thus, a new EWOD DMF design was attempted to test the effect of gel size reduction on gel formation time. The smaller gel size would also test to see if liquid could flow around the gel during excess liquid separation instead of being blocked by the gel.

4.2.2 Design and Fabrication

A smaller gel was sought to be made by embedding a smaller gel formation site electrode inside a regular size electrode. Circular gel formation sites were chosen in the hopes of producing circular gels that would provide the least resistance to the flow of liquid around the gels. In order to create the smaller gel, a means to deliver a smaller volume of sodium alginate to the gel formation site would be required. This was done by incorporating a dedicated flow pathway exclusively for sodium alginate and composed of smaller 1mm x 1mm electrodes that could deliver the reduced volume of sodium alginate to the gel formation site. Then, calcium chloride could be delivered through the regular 2mm x 2mm size electrodes to the gel formation site where it would surround the sodium alginate drop and merge with it resulting in gel formation.

This design layout is shown in Figure 4-1 where the sodium alginate flow pathways and calcium chloride flow pathways are clearly labeled as well as the location of a circular gel formation site. The radius of the circular gel formation site was determined by equating the area of a circle that held the same area as a 1mm x 1mm square electrode, which resulted in a value of 0.56 mm. The EWOD DMF mask that was designed incorporated 4 gel formation sites and corresponding flow pathways so as to enable the formation of 4 separate alginate hydrogels.

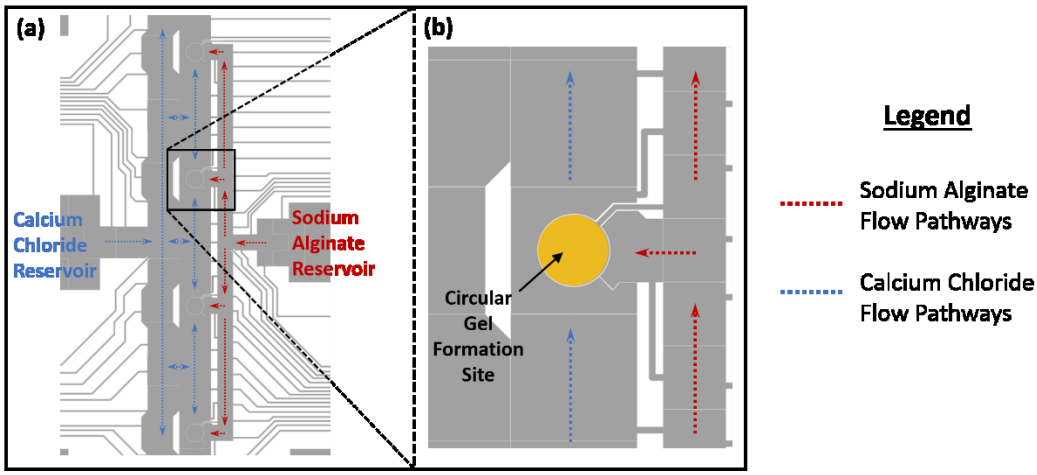

Figure 4-1 (a) Portion of EWOD mask used for Design A showing location of 1mm x 1mm Sodium Alginate flow pathways and 2mm x 2mm $CaCl_2$ flow pathways as well as their respective reservoirs. (b) Zoomed in section of (a) showing one circular gel formation site (highlighted by yellow circle for emphasis) of radius 0.56 mm.

EWOD DMF devices were fabricated and operated in the manner previously described in sections 2.2 and 2.3 using the mask described above.

4.2.3 Experimental Protocol

0.5% wt/vol sodium alginate solutions and 100 mM calcium chloride solutions were prepared in the same way described as in section 3.4.2. Gel precursors were loaded in to their respective reservoirs and the cover slip was mounted on 100 μm spacers placed on the base EWOD device.

For testing gel formation, first, sodium alginate drops were dispensed from the dedicated sodium alginate reservoir and transported to the gel formation site. Four such drops could be delivered per device since each device had 4 gel formation sites.

Once the sodium alginate drops were in place at the gel formation sites, calcium chloride drops were dispensed and brought to the gel formation site. There they were merged with the sodium alginate drop at the gel formation site and allowed to gel. After

allowing time for gelation (times ranging from 5 to 15 minutes), excess liquid separation was attempted and the shape of the gels formed were noted. The specific protocol is explained using electrode numbers as shown in Figure 4-2.

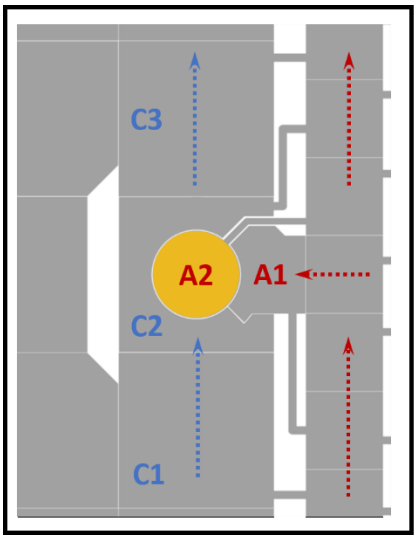

Electrode Numbering Legend

A1 – Sodium alginate electrode (1mm x 1mm) adjacent to gel formation site

A2 – Circular gel formation site electrode (r=0.56mm)

C1 – Main flow path electrode (2mm x 2mm) delivering calcium chloride to C2

C2 – 2mm x 2mm electrode encapsulating gel formation site A1 through which calcium chloride is delivered to A1

C3 – Calcium chloride electrode (2mm x 2mm) for extracting excess liquid from gel formed on A1

Figure 4-2 Electrode numbering map to illustrate protocol for gel formation on Design A

The specific protocol used while forming gels and removing excess liquid is as follows. First, sodium alginate is dispensed from its parent reservoir and transported through dedicated sodium alginate flow paths (1mm x 1mm pathways) all the way to electrode A1 which delivers the drop to the final gel formation site at electrode A2. Then, a calcium chloride drop is brought through the main flow path electrodes (2mm x 2mm pathways) to electrode C1. Then, while keeping electrode A2 on to keep the sodium alginate drop in place, electrode C1 is turned off while simultaneously electrode C2 is turned on. This allows the calcium chloride drop to move to the gel formation site and merge with the sodium alginate drop. Once sufficient time has been provided for gelation to occur, excess liquid removal is attempted. This is done by first turning on electrodes A2 and C2. Then electrode C3 is turned on and C2 is turned off, while A2 is still kept on.

If needed the electrode next to C3 is also actuated and in this manner, excess liquid separation is attempted while trying to keep the gel on A2.

4.2.4 Results and Discussion

Attempts at gel formation using this new design were only sporadically successful in forming gels and removing excess liquid. An example of this is seen in Figure 4-3 which shows how a calcium chloride drop is merged with the sodium alginate drop and after gelation, excess liquid removal is carried out leaving behind a calcium alginate hydrogel at the gel formation site.

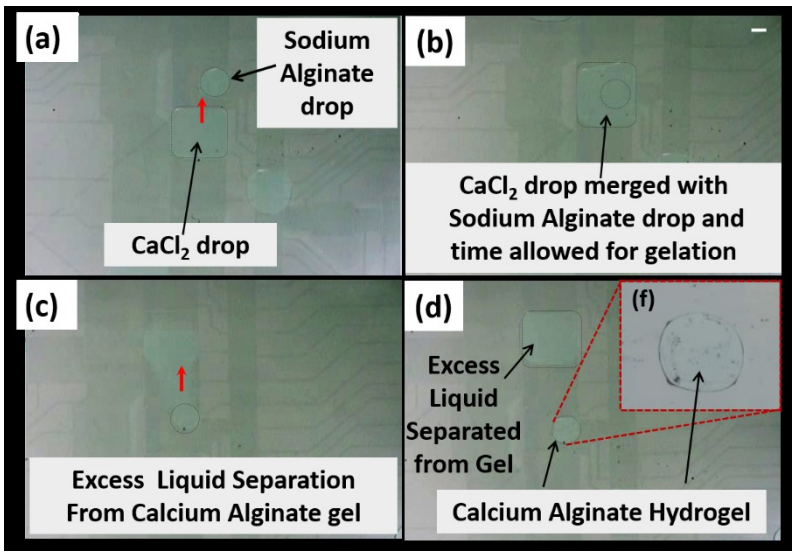

Figure 4-3 (a) Zoomed in section of EWOD layout used for hydrogel formation by encapsulation method. Blue lines show pathways for delivery of other liquids (calcium chloride, culture media, etc.) to the gel. (b)-(e) show the method of gel formation. Initially, a calcium chloride drop is brought to the sodium alginate drop which has already been delivered to the gel formation site as seen in (b). Once in position, the electrode surrounding the target gel site is activated as seen in (c) and calcium chloride encapsulates and merges with sodium alginate. After allowing 7 minutes for gel formation, excess liquid separation is carried out as seen in (d) and (e). The inset (f) shows a magnified view of the gel post that is formed in this process. Scale bar represents 500 μm

However, the above example showing a successful result was not very common and more the exception than the norm. The circular gel formation sites failed to ensure that circular gels were formed as can be seen below in Figure 4-4.

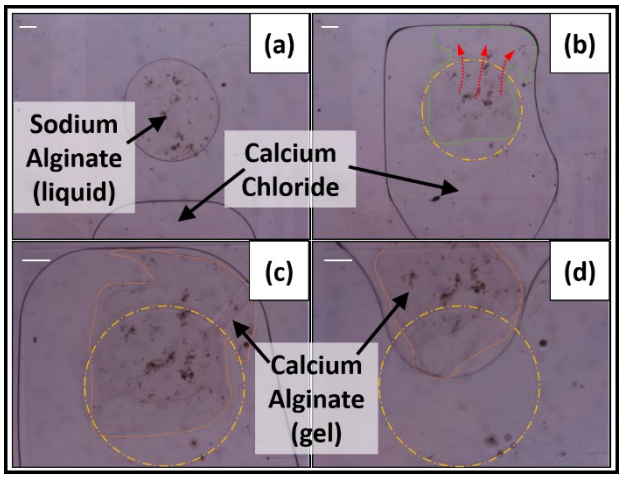

Figure 4-4 Figure shows snapshots taken from a video recording showing an attempt at gel formation with the design shown in Figure 4-1. Initially, a calcium chloride drop is brought adjacent to the gel formation site which is turned on and occupied by sodium alginate as seen in (a). When the intermediate electrode is activated, calcium chloride flows to surround the sodium alginate drop, but the sodium alginate drop also flows out of the gel formation site in the direction as shown by the red arrows in (b). The green dotted line traces the outline of the now displaced sodium alginate drop. Image (c) shows a magnified view of the system after 10 minutes has been provided for gel formation. The orange dotted line shows the outer boundary of the hydrogel which clearly lies partly outside the original gel formation site as shown by the yellow dotted circle. Image (d) depicts how the gel formed (red dotted boundary) gets displaced and dragged along with the excess liquid when excess liquid separation is attempted. Scale bar represents 100 μm

The sodium alginate drop starts off as being circular since it takes the shape of the gel formation site. However, when calcium chloride is brought to the gel formation site, it was observed that the calcium chloride drop merged with the sodium alginate drop before it completely encapsulated the sodium alginate drop. At the instant of merging, the exposed sodium alginate boundaries formed a thin layer of calcium alginate gel. But

before further gelation could occur, the momentum of incoming calcium chloride was sufficient to push the alginate out of the gel formation site and into the surrounding electrode. This resulted in the ungelled sodium alginate being pushed to the boundary edge where it then eventually became a gel through the diffusion of calcium ions into the alginate system. This resulting gel was found to be irregular in shape and not centered on the gel formation site but in between the main flow path electrodes.

The problem with this frequently occurring situation was not just limited to irregular shaped gels which were clearly non circular, but also affected excess liquid separation. Since the gel would end up displaced and not centered on the gel formation site, during excess liquid separation attempts, the gel would get caught in the location where necking should have occurred. Since the gels presence prevented necking, the net effect of attempting excess liquid separation was a tug of war between the main flow pathway electrode and the gel formation site electrode. Since the gel formation site was the smaller electrode, the force exerted by the gel formation site was less than the force exerted by the main flow pathway electrode. This resulted in the entire droplet and gel being carried away to the main flow pathway electrode instead of drop separation occurring.

It was clear from repeated experiments that just reducing the gel formation site and using circular electrodes was not sufficient to produce uniform gels of uniform shape from which excess liquid could be separated.

4.2.5 Conclusion

Design A was tested and found to fall short mainly due to the displacement of sodium alginate out of the gel formation site during merging with calcium chloride. This resulted in irregular shaped gels that were formed away from their intended locations. Having a means to hold or anchor the sodium alginate and calcium alginate in place

during the merging process with calcium chloride could possibly remedy this issue and result in the uniform gels that were sought to be obtained.

4.3 Hydrophobic Patterning of Circular Gel Formation Electrodes (Design B)

4.3.1 Objective

Based on the conclusions of testing Design A discussed above, the need for a suitable means to anchor and hold the sodium alginate in place during the merging process with calcium chloride became apparent. Eydelnant et al [102] reported a method to create hydrophilic “virtual microwells” on EWOD DMF to serve as a means for passive dispensing of reagents. These hydrophilic spots were created by lift off patterning of the hydrophobic Teflon layer on EWOD DMF and provided a means to dispense precise volumes of liquid without the need for a backing force. Adapting this method to Design A discussed above by hydrophilic patterning of the gel formation site was therefore attempted as a means to hold the sodium alginate in place during calcium chloride merging and also to anchor the gel formed so that the problems faced in Design A could be overcome.

Teflon lift off would expose the sodium alginate to direct contact with the dielectric Su8 layer. The contact angle for water with Su8 is much lower than the decrease in contact angle experienced by water when subjected to EWOD actuation on a Teflon surface. Therefore, EWOD actuation would not be able to exert greater force than the hydrophilic attraction that water or aqueous liquids would experience by virtue of the hydrophilic patterning.

4.3.2 Design and Fabrication

Since this approach was a modified version of the previous Design A, the basic mask layout remained the same. The only difference lay in the extra step of hydrophilic patterning (by Teflon lift off) of the gel formation sites as shown in Figure 4-5.

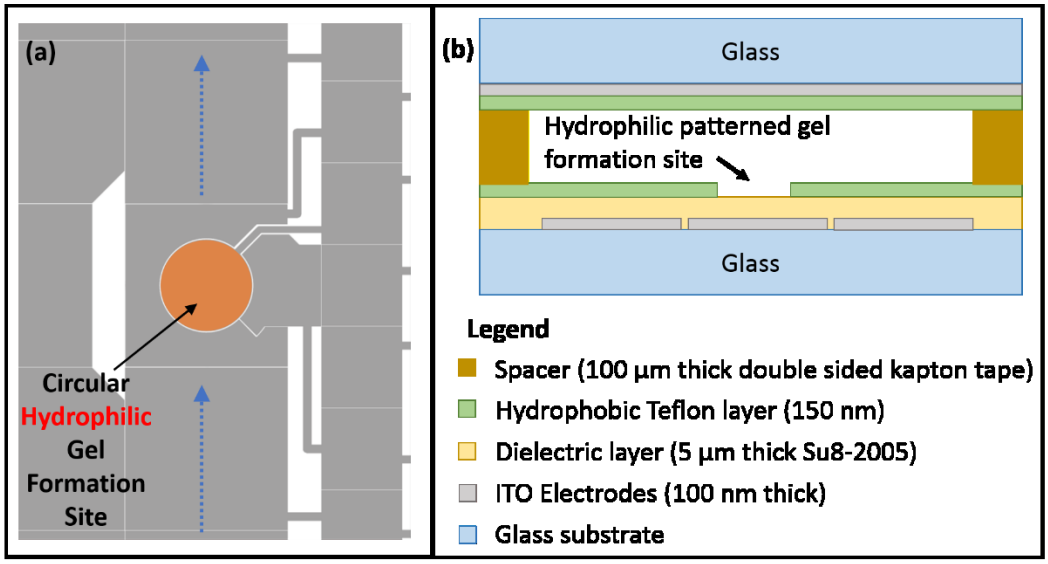

Figure 4-5 (a) Top view of EWOD layout showing location of hydrophilic circular gel formation site. (b) Side view schematic (not to scale) of assembled EWOD device showing different layers. Hydrophilic patterning of gel formation site is done by Teflon lift off process that creates an opening in the hydrophobic Teflon layer.

The basic fabrication of Design B is the same as Design A with the only difference being in the last stage of Teflon coating of the bottom EWOD chip. To carry out the Teflon lift off, the process similar to that adopted by Eydelnant et al [102] was adopted. Shipley 1813 positive photo resist was spin coated and photolithographically patterned over the dielectric Su8 layer such that after developing, circles of S1813 remained over the gel formation sites. This Su8 layer was then flood exposed for 30 seconds before hard baking at 150°C for 5 minutes. Then, a dilute 1% Teflon solution was spin coated over the EWOD device and baked at 95°C for 5 minutes. Teflon lift off was then carried out by rinsing the EWOD device with acetone until the S1813 circles patterned over the gel formation sites were removed, lifting off the Teflon above it in the process. This took ~ 5 minutes of agitation. Following this, the device was rinsed, dried and dehydrated at 150°C for 5 minutes.

Apart from the Teflon lift off step, all other steps for fabrication and device operation remained the same as that described in section 2.2 and 2.3.

4.3.3 Experimental Protocol

The protocol adopted for testing out Design B was the exact same as that used in Design A (section 4.2.3) except for actuation of the gel formation site electrode. Since the gel formation site electrode was now hydrophilic with respect to the surrounding hydrophobic surface, providing actuation to the gel formation site electrode was redundant and unnecessary. The only time it was actuated was when sodium alginate was initially delivered to the gel formation site. Once the hydrophilic gel formation site was occupied by sodium alginate, no further actuation of the gel formation site was needed.

4.3.4 Results and Discussion

Sodium alginate drops were dispensed from a reservoir and delivered to the hydrophilic gel formation site through a dedicated alginate transport pathway. A regular 88 V_{rms} at 1 kHz EWOD actuation voltage was used. Circular drops of sodium alginate (liquid) were formed at the gel formation site due to the circular hydrophilic sites. Calcium chloride was then brought to the gel formation sites and calcium alginate gelation was allowed to occur for ~ 10 minutes (compared to 15 minutes provided for larger gels in initial experiments carried out in chapter 3) before excess liquid separation was attempted.

Repeated experiments revealed that the hydrophilic site for gel formation and anchoring was not a reliable approach as it faced similar issues to those observed using Design A. While the hydrophilic patterning ensured that liquid always occupied the gel formation site as shown in Figure 4-6, it could not differentiate between sodium alginate and calcium chloride. Thus, when the intermediate electrode surrounding the gel

formation site was turned on, a thin layer of calcium alginate hydrogel was instantly formed at the interface between sodium alginate and calcium chloride. The momentum of the incoming calcium chloride drop was transmitted through the thin calcium alginate hydrogel to the still liquid sodium alginate, causing the incomplete gelled system to be displaced out of the hydrophilic site and towards the adjacent electrode as seen in Figure 4-6 (b). Since gelation was occurring during this displacement stage, the final result was a very irregular triangular shaped gel.

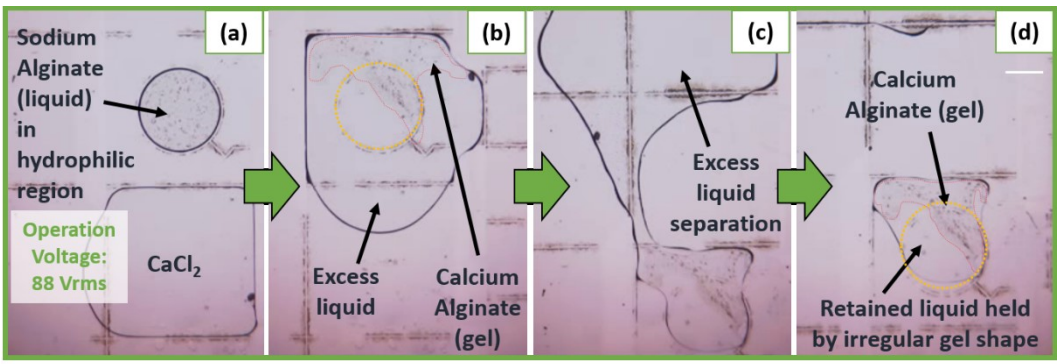

Figure 4-6 Snapshots of attempts (a-d) at gel formation in Device A using regular operating voltage (88 V_{rms}) resulting in highly irregular gel shape (b-d). Red dotted lines have been added in (b) and (d) to allow easier visibility of the approximate boundary of alginate gel formed while yellow dotted circles show the position of the original hydrophilic site. Scale bar in (d) represents 0.5 mm

Although excess liquid separation was possible as evidenced in Figure 4-6 (c)-(d), the shape of the gel ensured that residual liquid (with volume ~ equal volume of the gel) remained trapped by the gel and the hydrophilic patterned site. This was already described as an undesirable phenomenon in the alginate gelation section.

In order to reduce the sodium alginate displacement by incoming calcium chloride, the entry velocity of calcium chloride into the intermediate electrode surrounding the gel formation site was reduced. This was accomplished by reducing the electrode actuation voltage since this is known to lower drop speed [103]. By reducing the

intermediate electrode voltage actuation from 88 to 53 V_{rms}, the velocity with which calcium chloride entered the intermediate electrode was reduced. This resulted in less displacement of sodium alginate by incoming calcium chloride as seen in Figure 4-7 (b) and a less irregular gel shape than that obtained in the previous case. However, the small amount of sodium alginate displacement still resulted in the gel being formed partly outside the hydrophilic gel formation site. This caused the entire gel to be carried away by the excess liquid during the excess liquid removal step as depicted in Figure 4-7 (c)-(d). The hydrophilic patterned site ensured that a drop of excess liquid remained in the place where the gel should have been secured.

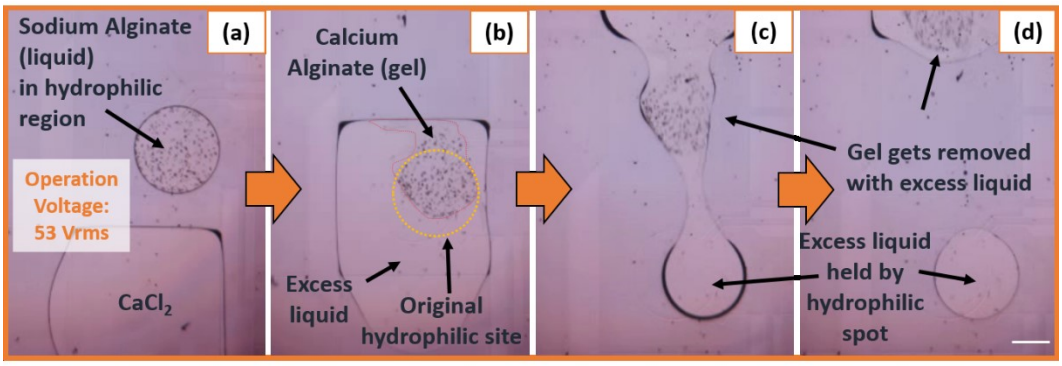

Figure 4-7 Gel formation and excess liquid separation attempt in Device B using reduced operating voltage (53 V_{rms}) resulting in gel anchoring failure as seen in (c)-(e). Red dotted lines have been added in (b) to allow easier visibility of the approximate boundary of alginate gel formed while yellow dotted circles show the position of the original hydrophilic site. Scale bar in (d) represents 0.5 mm.

The hydrophilic patterned gel formation site on their own did not result in an improvement in gel shape or gel anchoring and was deemed to be unsuitable for the purpose of a 3D tissue based chemical screening platform.

4.3.5 Conclusion

Based on the results of Design B, hydrophilic patterning of the gel formation sites was not able to reliably produce gels of regular shape that could be anchored or held in place during excess liquid separation. Although the hydrophilic patterning does ensure that liquid is always present on the gel formation site, it cannot distinguish between liquid and gel. Due to the momentum of incoming calcium chloride during the merging with sodium alginate, any gel that gets formed gets displaced from the original gel formation site. Reduction of this momentum helped result in better gel shapes but even slight displacement from the gel formation site was sufficient to cause loss of anchoring during excess liquid separation.

Thus, in order to develop a reliable gel formation design, a method has to be developed in which merging between the two gel precursors happens with as little momentum transfer as possible.

4.4 Encapsulation Using Separator Ring (Design C)

4.4.1 Objective

Based on the conclusions of the previous section (section 4.3.5), it was apparent that a design needed to be developed which allowed for merging of the sodium alginate and calcium chloride to occur without any displacement of the sodium alginate and resulting calcium alginate gel from the gel formation site.

In the previous designs tested (design A and B), it was noticed that calcium chloride merged with sodium alginate before calcium chloride had a chance to fully encapsulate or surround the sodium alginate. This resulted in poorly defined gel shapes as well as displacement of the gels from the gel formation site.

If this encapsulation step could be separated from the merging step, such that complete encapsulation of sodium alginate by calcium chloride occurred first before complete merging, then the momentum transfer would be minimized. This would also result in a gel whose external boundary would be defined immediately at the moment of merging taking care of gel shape.

In order to separate the encapsulation step (i.e. surrounding of sodium alginate drop with calcium chloride) from the merging step (i.e. merging of sodium alginate and calcium chloride to initiate gel formation), the use of a separator ring was proposed. The separator ring is a very thin electrode that surrounds the circular gel formation site electrode and separates it from the outer calcium chloride encapsulation electrode. Thus, the separator would provide an extra element of control over gel formation since it would prevent merging of the calcium chloride from the sodium alginate during the encapsulation step.

4.4.2 Design and Fabrication

The mask design for the encapsulation design using a separator ring electrode is shown below in Figure 4-8. This mask consisted of two different types of electrodes for fluid delivery – a larger 2mm x 2mm electrode flow pathway for calcium chloride and a smaller 1mm x 1mm electrode flow pathway dedicated for sodium alginate. The Gel Formation Site of radius 560mm was surrounded by a Separator Ring Electrode of thickness 30 μm. This Separator Ring Electrode was surrounded by the Encapsulating Electrode which had an inner radius of 600mm and outer radius of 1250mm. The Encapsulating Electrode could not completely encapsulate the Gel Formation Site due to the presence of a sodium alginate delivery electrode that had direct access to the Gel Formation Site. This direct access of sodium alginate to the gel formation site was

required to be able to deliver the smaller volume of sodium alginate to the gel formation site. The calcium chloride drop was intended to only reach the encapsulating electrode and did not need direct access to the gel formation site. All electrodes were separated by a gap of 10 µm.

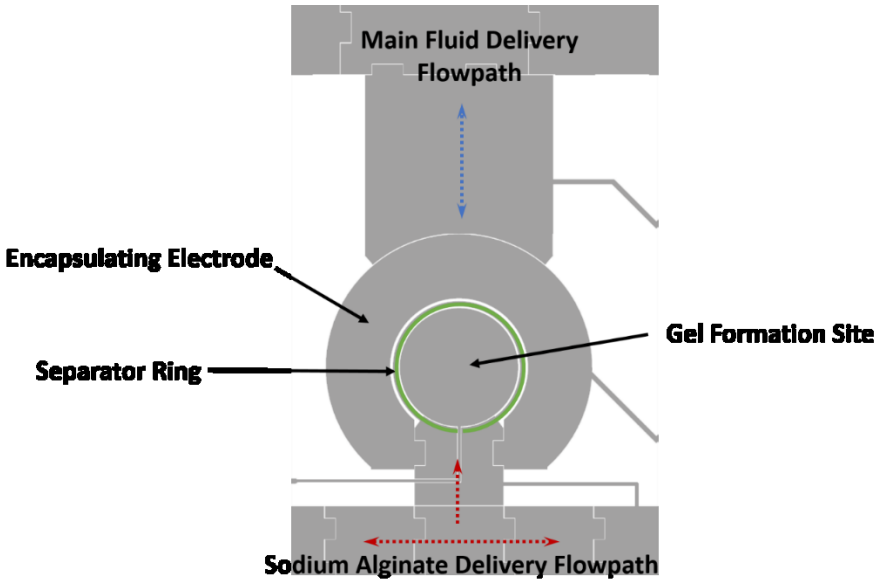

Figure 4-8 EWOD design showing encapsulation design with gel formation site, separator ring, encapsulating electrode and dedicated flow pathways for sodium alginate and calcium chloride.

EWOD DMF devices were fabricated and operated in the manner previously described in sections 2.2 and 2.3 using the mask described above.

4.4.3 Experimental Procedure:

Using this mask, devices were fabricated and basic gel formation experiments were attempted. 0.5% sodium alginate and 100 mM calcium chloride were loaded in their respective reservoirs. Sodium alginate drops were dispensed and delivered to the gel formation site. Then calcium chloride drops were dispensed and brought through the

main delivery flow path to the Encapsulating Electrode. Actuation of the separator ring was the means by which merging of calcium chloride and sodium alginate would be initiated. After allowing suitable time for gelation, excess liquid was separated by actuating the encapsulating electrode and drawing liquid to the main electrode flow pathway. While the main electrode flow pathway was kept on, the encapsulating electrode would be turned off and the gel formation site electrode turned on so that excess liquid could be pinched off and separated.

4.4.4 Results and Discussion

Based on repeat experiments, different phenomena were observed. While the separator ring was good in theory, another issue was identified which prevented the separator ring from performing as designed. This was the volume of liquid dispensed from the sodium alginate reservoirs and transported to the gel formation site. In cases where sodium alginate drop volume dispensed from the reservoir was the same as the volume of the gel formation site, the encapsulation design with separator ring worked well and allowed uniform gel formation as well as excess liquid removal. However, this was more the exception than the norm since most of the time, the sodium alginate drops dispensed by the reservoir were larger than the gel formation site volume.

Conventional reservoirs have already been identified as having upto 30% inaccuracy in volume dispensing in EWOD DMF [104]. This is accentuated even more so in the case of viscous liquids which tend to form longer necks on EWOD DMF during drop splitting and dispensing. The longer necks after splitting get consolidated partially within the dispensed drop and also with the reservoir drop. This further throws off the volume of the dispensed drop and tends to make it larger than normal liquids.

When larger than expected volumes were dispensed by the sodium alginate reservoir and transported to the gel formation site, the sodium alginate drops would overflow beyond the gel formation electrodes and spill over to the separation ring electrode and the encapsulation electrode. This proved to interfere with the separator ring performance since when the encapsulating electrode was actuated to draw in calcium chloride, the excess sodium alginate that overflowed the gel formation site boundaries would prematurely cause merging to happen with the incoming calcium chloride.

4.4.5 Conclusion

From the results of testing the encapsulation design using separator ring, it was concluded that while the encapsulation ring with separator ring concept worked, another issue had to be tackled which was the issue of accurate volume dispensing of sodium alginate droplets from the EWOD reservoir.

4.5 Improved Encapsulation Using Separator Ring and Precision Dispensing(Design D)

4.5.1 Objective

While the encapsulation design using separator ring concept of Design C did help to provide an additional amount of control over gel formation, it was also determined that the volume of sodium alginate delivered to the gel formation site was an important factor that needed to be controlled. The dispensing of viscous liquids on EWOD DMF can lead to issues with consistency of the volume of liquid delivered, with errors in volume dispensing using conventional reservoirs approaching 30% [104]. This is even more pronounced in the case of viscous liquids since viscous liquids tend to form longer necks

before drop separation. The extra length of these necks get incorporated into the dispensed droplet leading to droplets that have larger volume than the base electrode.

Due to volume errors in dispensing sodium alginate from the sodium alginate reservoir, there was variability in the volume of sodium alginate delivered to the gel formation site. In cases where the volume of dispensed sodium alginate exceeded the volume of the gel formation site, the sodium alginate would overflow beyond the boundary of the gel formation site and even cover the separator ring. Due to this, successful encapsulation of sodium alginate with calcium chloride would not occur. Merging would occur before complete encapsulation resulting in the same issues associated with Design A and B.

In order to ensure that sodium alginate volumes delivered to the gel formation site were consistent and precise and did not overflow beyond the gel formation site boundaries, a change in design and protocol was proposed. Instead of dispensing a drop of sodium alginate and delivering it to the gel formation site, it was decided to dispense precise volumes of sodium alginate directly at the gel formation site. This also had the added benefit of eliminating the separate alginate delivery flow pathways all together.

To do this, an extra-large drop of sodium alginate would be dispensed from one of the regular flow pathways and brought to the gel formation site. From this larger drop of sodium alginate, a smaller drop of sodium alginate would be dispensed directly at the gel formation site resulting in sodium alginate drops that would be of the same volume as the volume contained in the gel formation site. This would avoid scenarios where sodium alginate overflowed beyond the gel formation site.

4.5.2 Design and Fabrication

In Device D seen in Figure 4-9 (a), an improved encapsulation method was proposed. This method sought to form smaller circular gels and anchor them in place on the basis of intelligent electrode design rather than resorting to the use hydrophilic patterning. A separator ring electrode (of thickness 30μm with additional 10 μm space on either side from adjacent electrodes) was employed to separate the smaller circular gel formation site (radius 0.56 mm) from the encapsulating electrode (outer radius 1.25 mm) by a total distance of 50 μm. This would allow calcium chloride to fully surround the sodium alginate at the gel formation without merging. Once fully surrounded and encapsulated by calcium chloride, actuation of the separator ring electrode would cause the calcium chloride to merge on demand with sodium alginate. The encapsulation method of gel formation was expected to produce more symmetrical and uniform gel shapes since the instantaneous merging of the entire outer boundary of the sodium alginate drop with calcium chloride would immediately define the outer gel boundaries into a circular shape. This would thus eliminate any chance of irregular gels being formed due to premature electrode activation.

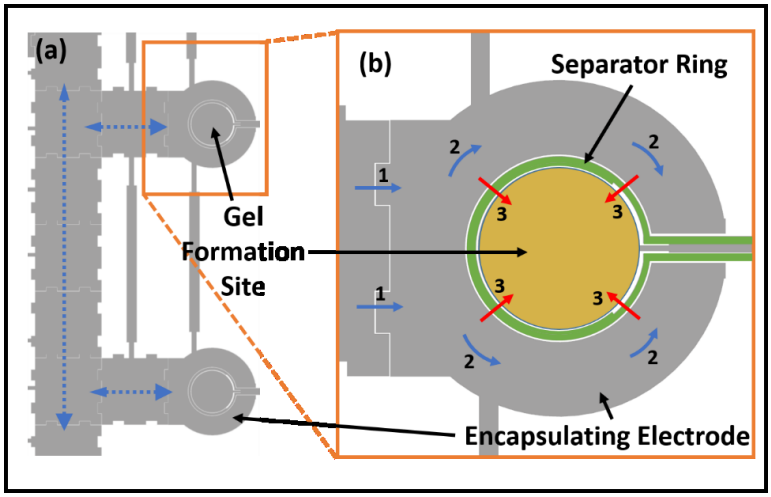

Figure 4-9 Image (a) shows a magnified section of the EWOD mask design used for the improved encapsulation design (Design D). Blue dotted arrows show the pathways for fluid transport on 1.9 mm x 1.9 mm electrodes. Inset magnified image (b) shows the separator ring electrode (in green) that allows for on demand merging of the calcium chloride with sodium alginate. Blue arrows with numbers show how calcium chloride should enter the encapsulating electrode (1) and then encapsulate the gel formation site (2). Actuation of the separator ring electrode causes calcium chloride to flow into and merge with the sodium alginate at the gel formation site as shown by red arrows (3).

The other change made in the improved encapsulation design as can also be seen in Figure 4-9 is the absence of a separate alginate delivery pathway since the new protocol described in section 4.4.2 was adopted for this design.

EWOD DMF devices were fabricated and operated in the manner previously described in sections 2.2 and 2.3 using the mask described above.

4.5.3 Experimental Protocol

0.5% wt/vol sodium alginate solutions and 100 mM calcium chloride solutions were prepared in the same way described as in section 3.4.2. Gel precursors were loaded in to reservoirs and the cover slip was mounted on 100 μm spacers placed on the base EWOD device.

For testing gel formation, first, larger drops of sodium alginate were dispensed from its parent reservoir and transported to the gel formation site. To get to the Gel Formation site Electrode (GFE) as seen in Figure 4-10, the large alginate drop was first transported through regular fluid delivery electrodes E1 and E2 to the Encapsulation electrode E3. Once at E3, the large alginate drop was brought to the gel formation site by simultaneous actuation of the Separator Ring Electrode (SRE) and GFE. To dispense a precise volume of sodium alginate at the GFE, the electrodes E2 and GFE were turned on. Further backing force was applied by actuation of electrode E1. Remaining sodium alginate drop was transported back to the sodium alginate reservoir.

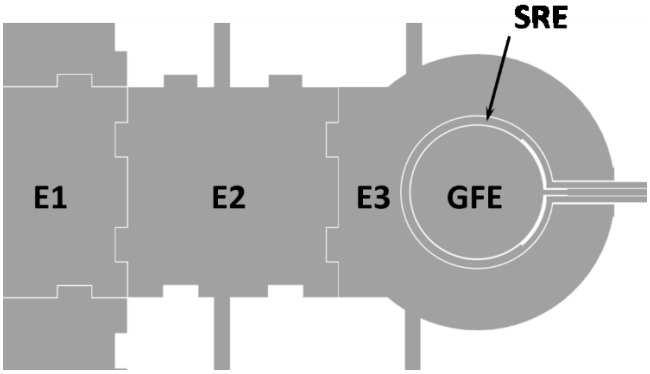

Figure 4-10 Image showing reference names of electrodes used in the gel formation process. E1 and E2 are fluid delivery electrodes of dimension 1.9 mm x 1.9mm. E3 is the Encapsulating electrode, while SRE and GFE are the Separator Ring Electrode and the Gel Formation Electrode respectively.

For gel formation, calcium chloride was dispensed from its parent reservoir and then brought through electrodes E1 and E2 to the Encapsulating Electrode E3. GFE is turned on at the same time as E3 to ensure that the sodium alginate in the GFE remains held in place. Once the calcium chloride has completely filled E3, then the SRE is turned on so that merging of the sodium alginate and calcium chloride occurs.

After allowing suitable time for gel formation, excess liquid separation is carried out. For excess liquid separation, the GFE is kept on all the time to ensure the gel remains in place. Then E3 and E2 are simultaneously turned on to draw the excess liquid away from the GFE. Once liquid has reached E2, then E3 is turned off and E1 is turned on to allow for extra backing force. In this manner, excess liquid gets pulled and separated from the gel which is held by GFE. Once the excess liquid has been separated, GFE is turned off and then excess liquid is transported to waste reservoirs through normal EWOD actuation sequences.

Using the above protocol, 4 discrete gel posts could be formed on a single post. Experiments were carried out to test the repeatability of gel formation and the ability to remove excess liquids.

4.5.4 Results and Discussion

Testing the improved encapsulation design (Figure 4-9) using the protocol described above demonstrated that this design was robust and repeatable in forming uniformly circular gels of consistent shape and size from which liquids could be repeatedly extracted.

In order to obtain precise volumes of sodium alginate contained within the gel formation site, the dispensing of sodium alginate directly at the gel formation site was carried out using the protocol described in the previous section. Snapshots from a video recording of an experiment depicting gel formation using Design D are shown in

Figure 4-11. Steps (a)-(c) clearly show how the precision dispensing is carried out. This precision dispensing at the gel formation site eliminated any possibility of sodium alginate flowing outside of its designated gel formation site during actuation of the encapsulating electrode or the separator ring.

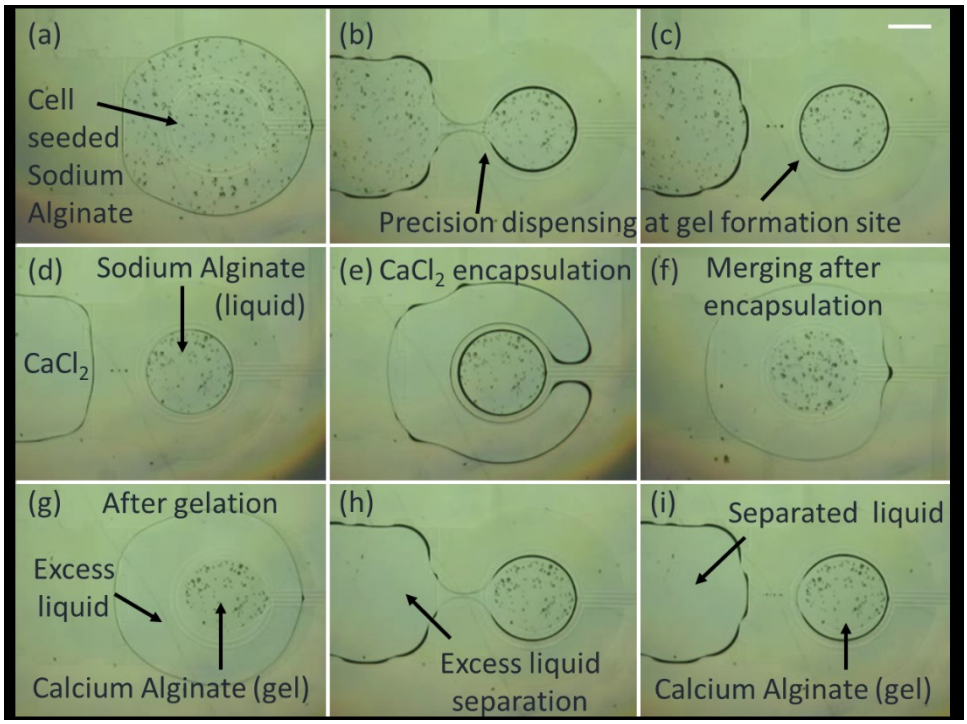

Figure 4-11 Images showing sequence of alginate gel formation. First, a precise volume of cell-seeded sodium alginate is dispensed at the target site as seen in (a)-(c). Then a calcium chloride drop is brought to the cell seeded sodium alginate drop and encircles it without merging (d)-(e). Actuation of the separator ring causes the two liquids to merge (f) in such a way that the sodium alginate drop is encapsulated by calcium chloride resulting in a circular gel shape. After sufficient time for gelation, calcium alginate hydrogels are formed and excess liquid is removed from the calcium hydrogel as shown in (g)-(i). Scale bar in (c) represents 0.25 mm

Precision dispensing of viscous liquids can be challenging on EWOD DMF but because of the nature of the circular electrode and the distance of separation from the backing electrode E2, the neck formed was very small and splitting of the drop resulted without the sodium alginate overflowing beyond the gel formation site electrode boundaries.

Following the precision dispensing of sodium alginate, calcium chloride was brought to the encapsulating electrode where it fully encapsulated the sodium alginate at the gel formation site without merging in the process as seen in

Figure 4-11 (d)-(f). Once complete encapsulation was achieved, the separator ring was actuated which allowed for the controlled merging of the inner sodium alginate drop with the outer calcium chloride drop. Since the separator ring only separated the two drops by a total distance of 50 μm, there was little fluid flow and momentum transfer and the overall gel shape retained the circular shape of the gel formation site electrode. Also, no displacement of the sodium alginate was observed from the gel formation site and the resulting calcium alginate hydrogels always formed at the circular gel formation site. This ensured that the gel always remained in place during excess liquid removal and never got carried away with excess liquid. Since no barrier or hydrophilic patterning was required to retain the gel in place unlike other EWOD DMF devices reported for hydrogel based 3D cell culture and screening [82,83], this design proved to be easy to fabricate and implement and offers a simple solution not just for alginate hydrogels but any other hydrogel based system.

Using the improved encapsulation method, calcium alginate hydrogels could be formed of consistent and symmetrical circular shape between different gel formation sites on the same device as well as across multiple devices. The circular shape of the alginate hydrogel provided minimal resistance to the removal of excess liquid as seen in

Figure 4-11 (g)-(i). This new encapsulation method ensured that alginate hydrogels could be created in a convenient and fast manner requiring a gelation time of only 5-7 minutes and that excess liquids could be removed and new liquids added without loss of gel integrity or gel displacement.

4.5.5 Conclusion

The improved encapsulation design using the separator ring was tested and found to be successful in producing gels of uniform shape and size with a high degree of repeatability. The method of dispensing sodium alginate drops at the target gel formation site combined with improved encapsulation design using the separator ring was found to be successful in producing gels of uniform shape and size with a high degree of repeatability. Excess liquid could be separated from the gels without the use of additional anchoring methods and the gel always remained in place. This lays the foundation for a method to form cell seeded alginate hydrogels that can be incorporated into a 3D cell culture and chemical screening platform.

Chapter 5

Cell Culture and Chemical Delivery

5.1 Introduction

The previous chapter presented a design that was capable of forming uniform circular alginate gels that could allow reliable excess liquid removal. That design lays the foundation for a proof of concept EWOD DMF device capable of 3D cell culture and chemical screening which is covered in this chapter. Here, for a model 3D cell culture system, MCF-7 breast cancer cells in calcium alginate hydrogels were used. In order to demonstrate the chemical screening capability, dimethyl sulfoxide (DMSO) was chosen. DMSO is a common chemical used in biology labs for the cryopreservation of cells. However, at higher concentrations it is known to be cytotoxic and will kill cells. The cytotoxicity of DMSO on cells in a droplet was already carried out on EWOD DMF in a study by Park et al [78]. Here, we propose to use a similar methodology except extend it to 3D cell culture to see the effect of delivery of DMSO at different concentrations.

5.2 EWOD Design

A EWOD mask was created using L-Edit to allow for the formation of 4 discrete gel formation sites. It used the improved encapsulation design using separator ring electrodes to allow for the creation of stable and uniform gels that were capable of being addressed by various liquids. Figure 5-1 shows the layout of the mask complete with 6 different reservoirs for holding cell seeded sodium alginate, calcium chloride, culture media, DMSO, fluorescent dye, and a waste reservoir. A dedicated DMSO mixing and dilution area is also provided to enable for the dilution of DMSO to desired concentrations.

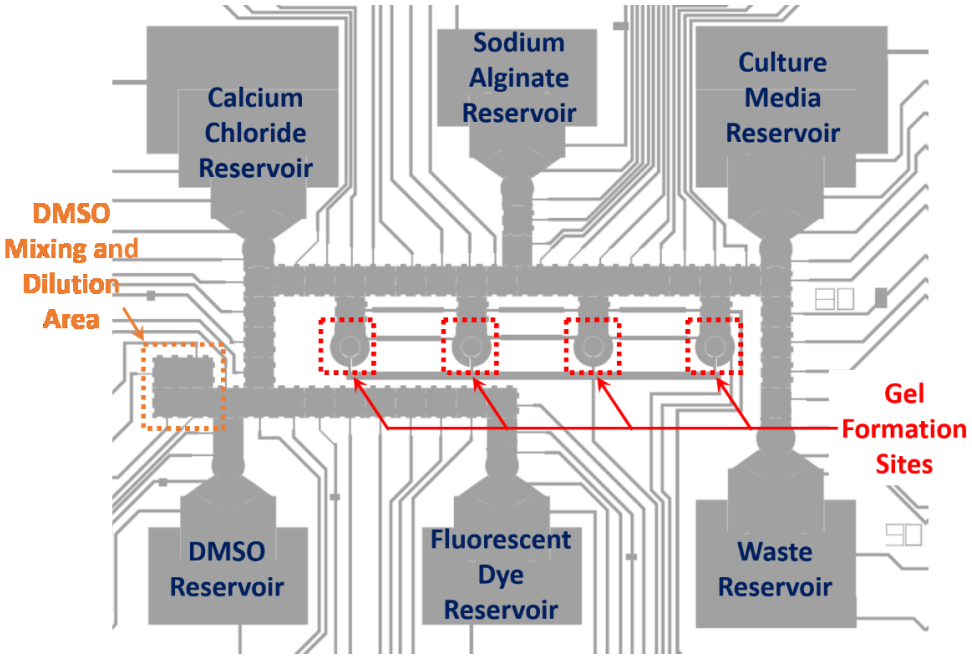

Figure 5-1 EWOD design for integrated cell culture and chemical screening showing location of reservoirs, DMSO dilution area and gel formation sites

5.3 Material and Methods

5.3.1 Cell Culture

Human breast cancer cells (MCF-7) obtained from American Type Culture Collection (ATCC) were maintained in culture medium (D-MEM/F12, Life Technologies, Carlsbad, CA), and supplemented with 4% fetal bovine serum, 2 mM l-glutamine, 100 µg/mL penicillin/streptomycin, and 0.01 mg/mL insulin. Cells were incubated in 25 cm2 T-flasks at 37°C and 5% CO2 while being sub-cultured every 3-4 days at ~ 80% confluency.

5.3.2 Cell Seeded Alginate Hydrogel Precursor Reagents Preparation

In order to prepare 0.5% wt/vol sodium alginate solutions, first stock solutions of sodium alginate were formed by dissolving low viscosity sodium alginate powder (Sigma Aldrich, St. Louis, MO – CAS 9005-38-3) in deionized water to obtain a concentrated 4% wt/volume sodium alginate solution. This concentrated alginate solution was diluted in a 1:4 ratio with MCF-7 cells suspended in DMEM/F12 to obtain a 0.5% wt/vol of cell seeded sodium alginate solution with a concentration of 0.5-1 x 10^6 cells/mL.

100 mM calcium chloride solutions were prepared by dissolving calcium chloride crystals (Sigma Aldrich) in DMEM/F12 culture media.

In order to prevent biofouling [65], pluronic F-68 was added to all culture media containing reagents at 0.04% wt/vol concentration.

5.3.3 Fluorescent Dye Preparation and Staining Protocol

Fluorescent dyes Hoechst 33342 (Life Technologies) was used to stain all the cells present in the hydrogels while Propidium Iodide (PI) (Life Technologies) was used to stain all the dead cells. H-33342 and PI were dissolved in sterile culture grade water to obtain final dye concentrations of 5ug/ml of H-33342 and 8ug/mL of PI.

5.3.4 DMSO Dilution and Delivery Protocol

DMSO solutions of different concentrations were prepared on EWOD chips through a serial dilution protocol similar to that used by Park et al [78]. A stock solution of DMSO was prepared by mixing sterile culture grade DMSO (Sigma Aldrich), deionized water, Hoechst-33342 and Propidium Iodide to obtain a 50% v/v DMSO solution with the same final dye concentration of H-33342 and PI as used to prepare the fluorescent dye solution described earlier. This stock solution was loaded into the EWOD reservoir. In order to obtain 25% DMSO solution, a drop of 50% DMSO stock solution was dispensed

from the reservoir and brought to a designated mixing zone where it was merged with another drop of fluorescent dye in a 1:1 volume ratio. Mixing was carried out by completing 5 rotations of the merged drops (where one rotation comprised of moving the drop over 4 electrodes in a counter-clockwise pattern). This yielded a 25% solution of DMSO that was split into 2 drops – one for delivery and the other for further dilution. Mixing the 25% DMSO drop with another drop of fluorescent dye in the same manner as discussed above (6 rotations) yielded a 12.5% DMSO solution from which one drop was dispensed while the other was sent to waste. In this manner, concentrations of 50%, 25% and 12.5% DMSO were obtained while the 0% concentration was a control drop of fluorescent dye. By using the above protocol, the fluorescent dye concentration remained the same across all the drops and the only variable that changed was the percentage of DMSO. Figure 5-2 below depicts a schematic of the first step in DMSO dilution that starts with a DMSO and fluorescent dye drop and results in a 50% diluted DMSO drop.

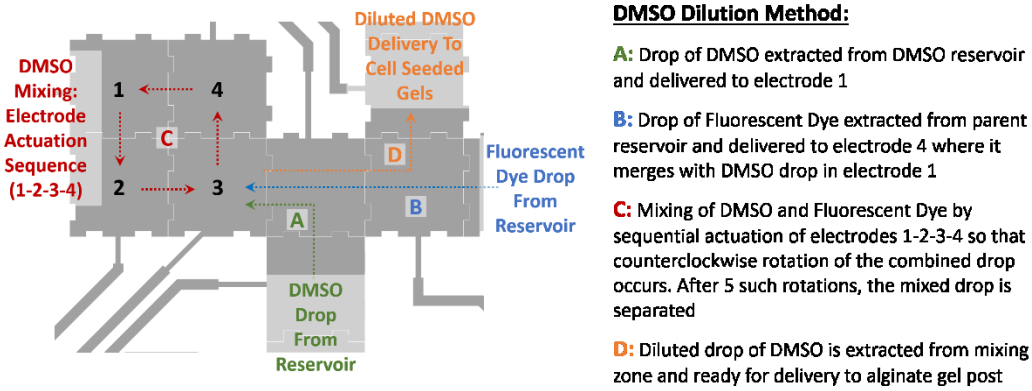

Figure 5-2 Schematic of DMSO dilution protocol on EWOD device

5.3.5 Viability and Targeted Chemical Delivery Experiment Protocol

In order to carry out the targeted drug delivery experiments, MCF-7 cell seeded alginate hydrogels were created at designated tissue post sites. This was done by dispensing cell seeded sodium alginate drops and delivered to designated tissue post

sites. Calcium chloride drops was similarly dispensed from its parent reservoir and brought to the tissue post sites where they were merged with sodium alginate drops and gelation was allowed to occur. During this gelation process, simultaneous preparation of different concentrations of DMSO (0%, 12.5%, 25%, and 50%) was carried out in another area on the same chip using the DMSO dilution protocol as described earlier. After allowing sufficient time for gelation (~7 minutes), excess liquid from the tissue posts was extracted and dispensed to waste. The 4 different DMSO solutions were then delivered to the target tissue posts and the whole chip was incubated for 30 minutes in a 37°C, 5% CO2 humidified incubator following which fluorescence images were then taken using the protocol described below.

5.3.6 Fluorescent Microscopy and Cell Counting

Fluorescence images were taken using fluorescence microscope (Olympus BX-51) to visualize the cells in the gel posts stained by the fluorescent dyes. H-33342 dye stained all the cells present blue when viewed under DAPI filters while dead cells were labeled red by PI dye when viewed under TRITC filters.

Fluorescent images thus obtained were combined using ImageJ (NIH) so that the dead cells labeled red were overlaid with all the cells present in the sample that were stained blue. The resulting image clearly allowed viable cells to be distinguished from dead cells.

For experiments where viability was measured, cell counting was carried out manually using combined fluorescent images and the cell counter plugin in ImageJ software. This yielded the total number of live and dead cells, which were then used to calculate the viability percentage. The targeted chemical delivery experiment was repeated 3 times and results were presented as viability percentage ±1 standard deviation.

5.4 Results and Discussion

To demonstrate the targeted chemical delivery abilities of this proposed screening platform, four MCF-7 seeded calcium alginate hydrogels were formed on chip as per the improved encapsulation method. While gelation was taking place, different concentrations of DMSO (0, 12.5, 25 and 50 %) were formed on chip as per the method described in the methods and material section. Once the calcium alginate hydrogel gelation was complete, excess liquid was removed and discarded to waste and the 4 different DMSO concentration drops were delivered to 4 gels and incubated for 30 minutes. Figure 5-3 shows one such result of such an experiment where cells were seeded at a high density to better allow visualization of the variation in cell. Based on the fluorescence images, a clear difference in viability of cells is observed with viability decreasing as DMSO concentration increases. Due to the high cell density used, this particular data set was not quantified and was only used for visualization purposes.

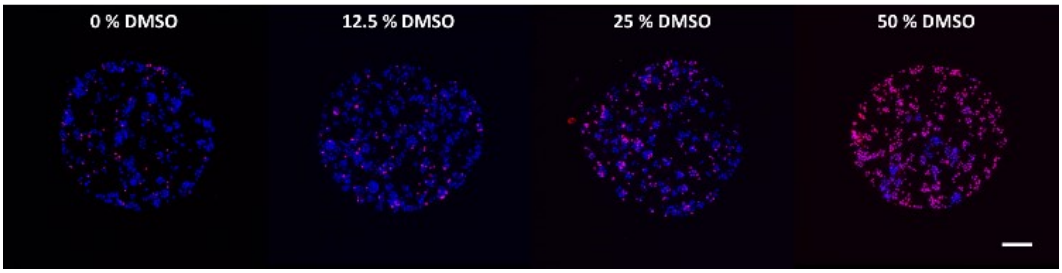

Figure 5-3 Effects of on chip DMSO delivery at 4 different concentrations (0%, 12.5%, 25% and 50%) to MCF-7 cell seeded calcium alginate hydrogel post. Hydrogels shown here were seeded at high cell density to allow for easy visualization of the variation in viability. These gels were stained with Hoechst-33342 and Propidium Iodide and the resulting fluorescent images were superimposed such that pink dots represent dead cells and blue dots represent viable cells. A clear increase in cell death can be visually observed as DMSO concentration increases. Scale bar represents 100 micron.

In order to determine the repeatability of this experimental procedure, 3 sets of the same experiment were carried out with cells seeded at lower density (in order to

facilitate counting of cells). The results of the replicate experiments are shown in Figure 5-4 which shows the variation in cell viability with exposure to 4 different concentrations of DMSO. The 0% DMSO concentration serves as the control gel to show the viability of cells formed on chip which are not exposed to any DMSO. The 12.5% DMSO gels showed a very slight decrease in viability compared to the control gels and this is to be expected since it is well known that exposure to low concentrations ~10% DMSO for short durations of time have a negligible effect on viability.

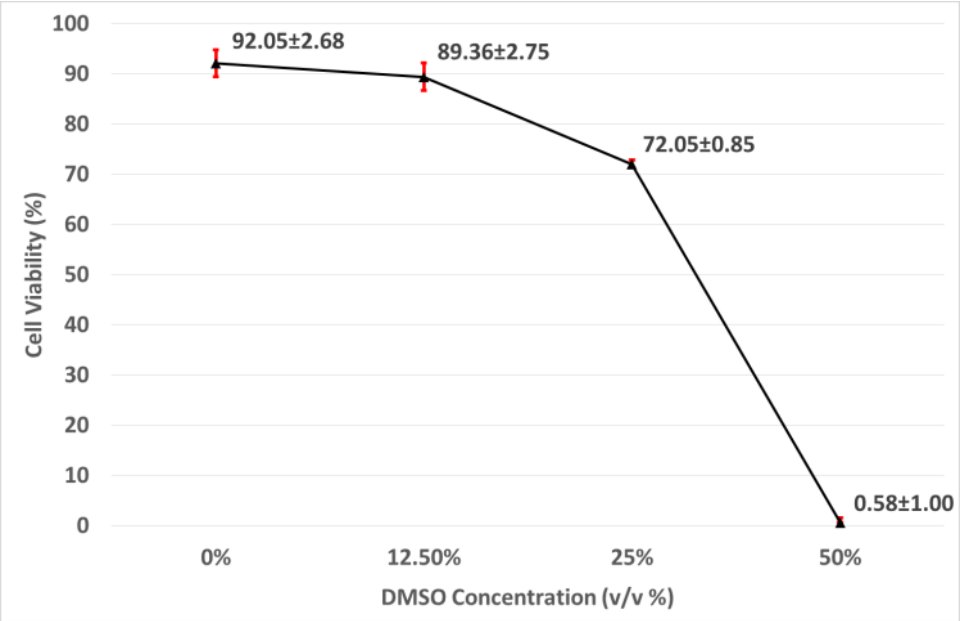

Figure 5-4 Plot showing how cell viability varied based on exposure to DMSO at various concentrations for 30 minutes. Cell viability at 12.5% DMSO concentration is only nominally lower than the control post exposed to 0% DMSO. However, as DMSO concentration increases, a clear dip is seen in viability at 25% and at 50% DMSO, virtually all the cells have died. Error bars (in red) represent ±1 standard deviation, n=3.

The gels exposed to 25% and 50% concentrations of DMSO show a marked decrease in viability with 25% DMSO concentrations showing a viability of 72.05% ± 0.85

while the 50% DMSO concentrations killing off all the cells in the 30 minute exposure time.

One notable result is the high degree of repeatability with the significantly small standard deviations when compared with the relatively high level of variation in biological experiments. This is attributed to the high degree of automation and robustness of the platform ensuring that variations arising from manual handling between experiments were kept to a minimum.

In order to demonstrate the ability to note changes in response of cells to DMSO over time, cell seeded alginate gels were formed on chip. While gelation was allowed to happen, different concentrations of DMSO (0%, 12.5% and 25%) were prepared on the same chip through serial dilution. Once gelation was complete and excess liquid was separated, the 3 different DMSO concentration drops were delivered to the tissue posts and the device was incubated. Fluorescent images were taken at 30 minute intervals to measure the effect of DMSO over a span of two hours on cell laden hydrogels. Figure 5-5 shows the resultant viabilities obtained at each time step for each gel post exposed to DMSO concentration. From the graph, it can clearly be seen that there is minimal decrease in viability of the cells in the control gel exposed to 0% DMSO. However a decrease in cell viability could be seen over the first 60 minutes for the 12.5% DMSO treated gel followed by no major increase in cell death at 90 minutes and 120 minutes. The 25% DMSO treated gel on the other hand showed a consistent increase in cell death at every 30 minute interval for the first 90 minutes with the cell death rate starting to taper off at 120 minutes.

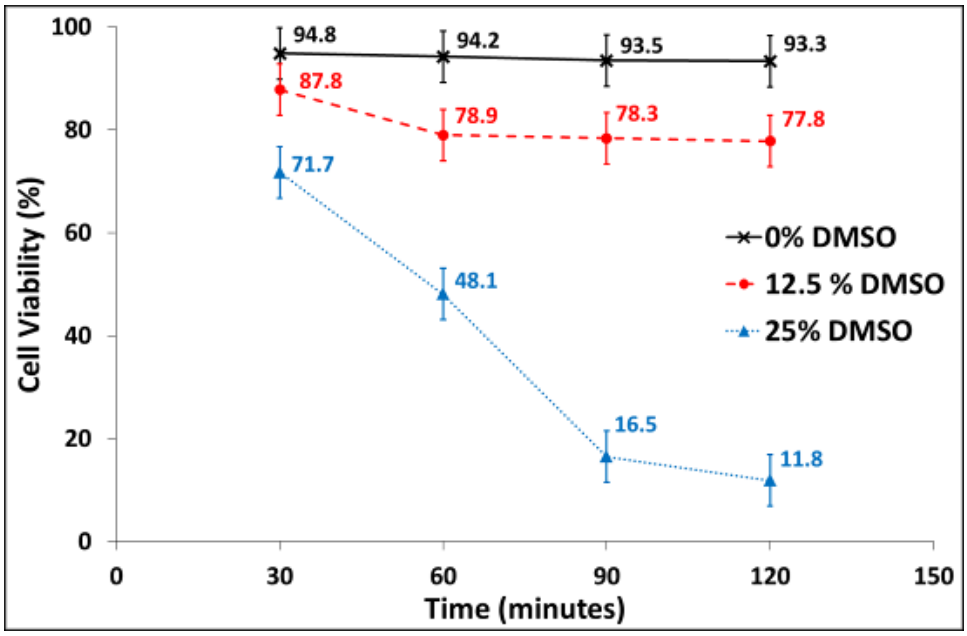

Figure 5-5 Plot showing time lapse variation in cell viability % during a single experiment (n=1) as hydrogels are exposed to varying DMSO concentration (0%, 12.5% and 25%) for 30, 60, 90 and 120 minutes. The cell-seeded gel exposed to 0% DMSO shows almost no increase in cell death over time. The cell seeded gel exposed to 12.5% DMSO shows an initial increase in cell death over the first 60 minutes but then stabilizes with no major increase in cell death at 90 minutes and 120 minutes of exposure. However the cell seeded gel exposed to 25% DMSO experience a sharp rate of cell death over the first 90 minutes before starting to taper off at 120 minutes. Error bars represent ±5% error to account for errors in cell counting

Such kinds of time-lapse experiments provide valuable insight into the effect of chemicals over time on cells without having to carry out multiple experiments. If images were only taken at a single time interval, then the only conclusion drawn would be that an increase in cell death occurs based on DMSO concentration exposure. Repeating the experiment with different time spans would show that cell death increases over time as well. However, being able to monitor the variation in cell death during the same experiment over time reveals that cell death in the 12.5% DMSO post increases only over the first 60 minutes and after that remains more or less constant. This kind of observation

relating the nature of cell death with both time and concentration would be hard to make using conventional experimental setups without having to carry out multiple experiments. The EWOD platform provides a simple and convenient means to take rapid images of multiple gel posts over multiple time frames with ease allowing investigators the ability to observe the transient effect of chemicals on cells cultured in a 3D environment.

5.5 Conclusion

The ability to maintain form hydrogels on chip with viable cells was demonstrated as can be seen from the viability of cells in the control post. The chemical screening capability was also showcased by using DMSO and diluting it to different concentrations and then delivering it to different cell seeded hydrogels on the same device. The effect of these different concentrations on viability was determined both for a fixed time scale as well as for varying amounts of time. Time-lapse results show how various concentrations of DMSO has a transient effect on cell viability.

Thus, the effectiveness of EWOD DMF for 3D cell culture and chemical screening applications has been demonstrated.

Chapter 6

Conclusions and Future Work

6.1 Conclusions

The ability to form calcium alginate hydrogels on EWOD DMF was investigated and demonstrated. For suitable use as a 3D cell culture and screening platform, consistently uniform gels are required to be formed that can be reliably addressed. Factors unique to alginate gelation on EWOD DMF that affect gel shape were identified such as the method of calcium chloride delivery and excess liquid removal before complete gelation. The necessity for excess liquid removal was realized and the importance of gel size, gel anchoring and gel shape were noted. A simplified diffusion model of alginate gelation was carried out which identified the effect that volume ratios and gel size had on the rate of calcium diffusion.

Based on all this information, various methods and designs were attempted to obtain uniform gel shapes on EWOD DMF from which excess liquid removal could be carried out. The adoption of circular gels of smaller size with respect to remaining fluid electrodes was not sufficiently able to retain gels in place. Hydrophilic patterning was attempted to try to retain and hold the sodium alginate in place during merging of calcium chloride but was found to be insufficient.

The momentum transfer from calcium chloride to sodium alginate was identified as a major factor responsible for displacing the calcium gels from the gel formation sites during gelation, resulting in irregular gel shapes that got carried away by excess liquid. In attempts to control and minimize this momentum transfer, a novel separator ring electrode design was proposed. During testing of the separator ring electrode, the need for precision dispensing of sodium alginate was realized. Dispensing accurate volumes of sodium alginate directly at the gel formation site was determined to be a viable solution

and incorporated into the EWOD DMF design and protocol. With this new protocol change, testing of the improved encapsulation design with a separator ring was carried out. This design proved to be robust and reliable, capable of forming uniform gels repeatedly across multiple gel formation sites and multiple devices. Circular gels were readily obtained and excess liquid separation was possible without the need for any kind of hydrophilic patterning or use of physical barriers to hold the gel in place.

This improved encapsulation design using a separator ring was then incorporated into a full-fledged device to test the 3D cell culture and chemical screening capability of EWOD DMF. MCF-7 cancer cell seeded alginate hydrogels were formed on 4 discrete gel formation sites on the EWOD DMF. DMSO was diluted to pre-determined concentrations on chip and delivered to gels formed on the same chip to investigate the effects of DMSO concentration based cytotoxicity on 3D cultured cells. A clear difference and progression of cell death was noted in DMSO concentrations at 25% and 50% while 12.5% DMSO only slightly affected cell viability. A time-lapse experiment was also carried out to demonstrate the combined effects of varying DMSO concentration and time of exposure on 3D cultured cells. The results of this experiment demonstrated clear variations in the transient cell death of cells when exposed differing concentrations of DMSO which would not have been realized otherwise.

Thus, a proof of concept platform for 3D cell culturing and chemical screening using EWOD DMF has been developed.

6.2 Recommendations for Future Work

Only short-term viability experiments able to be carried out. Long-term viability experiments were not feasible due to biofouling that was observed to occur, making drop motion sluggish and unmovable. However, with the use of improved pluronics, longer-term experiments might be possible and are worth investigating.

Hydrophilic patterning and the use of virtual microwells could pose an alternative solution to the biofouling problem. By patterning hydrophilic spots on the cover slip and aligning them with the gel formation post electrodes on the bottom EWOD DMF chip, hydrogels might adhere to the top cover slip. This would allow the bottom EWOD chip to be swapped out in case it was unresponsive due to protein deposition and resulting biofouling when conducting long-term experiments.

Increasing the number of gel formation sites would increase the practicality of the device. Only 4 gel formation sites were allocated on chip for this initial proof of concept study. However, the proposed design lends itself well to arraying without taking too much space and increasing the number of gels that can be handled is the logical next step to try in order to get more data points.

Alginate hydrogels were selected for their ease of gelation but the final design developed has potential to work with any kind of gel. Demonstrating the capability of the current EWOD DMF design to be compatible with any kind of hydrogel would greatly increase the attractiveness of this system since it would allow researchers flexibility in choosing their 3D cell environments.

DMSO is a known cytotoxic chemical at higher concentrations and was used here solely as a proof of concept application. Using more relevant chemicals or drugs that could possibly have metabolic effects on cells that would be more compelling evidence to the usefulness and versatility of EWOD DMF for 3D cell culture and screening applications.

References

[1] Pampaloni, F., Reynaud, E. G., and Stelzer, E. H. K., 2007, “The third dimension bridges the gap between cell culture and live tissue.,” Nat. Rev. Mol. Cell Biol., **8**(10), pp. 839–45.

[2] Gurski, L. A., Petrelli, N. J., Jia, X., and Farach-carson, M. C., 2010, “3D matrices for anti-cancer Drug testing and Development,” Oncol. Issues, **25**(February), pp. 20–25.

[3] Lee, P. J., Gaige, T. A., Ghorashian, N., and Hung, P. J., “Microfluidic tissue model for live cell screening.,” Biotechnol. Prog., **23**(4), pp. 946–51.

[4] Montanez-Sauri, S. I., Sung, K. E., Puccinelli, J. P., Pehlke, C., and Beebe, D. J., 2011, “Automation of three-dimensional cell culture in arrayed microfluidic devices.,” J. Lab. Autom., **16**(3), pp. 171–85.

[5] Tung, Y.-C., Hsiao, A. Y., Allen, S. G., Torisawa, Y., Ho, M., and Takayama, S., 2011, “High-throughput 3D spheroid culture and drug testing using a 384 hanging drop array.,” Analyst, **136**(3), pp. 473–8.

[6] Gómez-Sjöberg, R., Leyrat, A. A., Pirone, D. M., Chen, C. S., and Quake, S. R., 2007, “Versatile, fully automated, microfluidic cell culture system.,” Anal. Chem., **79**(22), pp. 8557–63.

[7] Gu, W., Zhu, X., Futai, N., Cho, B. S., and Takayama, S., 2004, “Computerized microfluidic cell culture using elastomeric channels and Braille displays.,” Proc. Natl. Acad. Sci. U. S. A., **101**(45), pp. 15861–6.

[8] Takayama, S., Ostuni, E., LeDuc, P., Naruse, K., Ingber, D. E., and Whitesides, G. M., 2003, “Selective Chemical Treatment of Cellular Microdomains Using Multiple Laminar Streams,” Chem. Biol., **10**(2), pp. 123–130.

[9] Leclerc, E., Sakai, Y., and Fujii, T., 2004, “Microfluidic PDMS (polydimethylsiloxane) bioreactor for large-scale culture of hepatocytes.,” Biotechnol. Prog., **20**(3), pp. 750–5.

[10] Hung, P. J., Lee, P. J., Sabounchi, P., Aghdam, N., Lin, R., and Lee, L. P., 2005, “A novel high aspect ratio microfluidic design to provide a stable and uniform microenvironment for cell growth in a high throughput mammalian cell culture array.,” Lab Chip, **5**(1), pp. 44–8.

[11] Pearce, T. M., Wilson, J. A., Oakes, S. G., Chiu, S.-Y., and Williams, J. C., 2005, “Integrated microelectrode array and microfluidics for temperature clamp of sensory neurons in culture.,” Lab Chip, **5**(1), pp. 97–101.

[12] Hattori, K., Sugiura, S., and Kanamori, T., 2011, “Scaffold fabrication in a perfusion culture microchamber array chip by O(2) plasma bonding of poly(dimethylsiloxane) protected by a physical mask.,” Biomicrofluidics, **5**(2), p. 22204.

[13] Li, L.-M., Wang, W., Zhang, S.-H., Chen, S.-J., Guo, S.-S., Français, O., Cheng, J.-K., and Huang, W.-H., 2011, “Integrated microdevice for long-term automated perfusion culture without shear stress and real-time electrochemical monitoring of cells.,” Anal. Chem., **83**(24), pp. 9524–30.

[14] Hung, P. J., Lee, P. J., Sabounchi, P., Lin, R., and Lee, L. P., 2005, “Continuous perfusion microfluidic cell culture array for high-throughput cell-based assays.,” Biotechnol. Bioeng., **89**(1), pp. 1–8.

[15] Kimura, H., Yamamoto, T., Sakai, H., Sakai, Y., and Fujii, T., 2008, “An integrated microfluidic system for long-term perfusion culture and on-line monitoring of intestinal tissue models.,” Lab Chip, **8**(5), pp. 741–6.

[16] Tourovskaia, A., Figueroa-Masot, X., and Folch, A., 2005, “Differentiation-on-a-chip: a microfluidic platform for long-term cell culture studies.,” Lab Chip, **5**(1), pp. 14–9.

[17] Lee, P. J., Hung, P. J., Rao, V. M., and Lee, L. P., 2006, “Nanoliter scale microbioreactor array for quantitative cell biology.,” Biotechnol. Bioeng., **94**(1), pp. 5–14.

[18] Zhang, B., Kim, M.-C., Thorsen, T., and Wang, Z., 2009, “A self-contained microfluidic cell culture system.,” Biomed. Microdevices, **11**(6), pp. 1233–7.

[19] Liu, L., Loutherback, K., Liao, D., Yeater, D., Lambert, G., Estévez-Torres, A., Sturm, J. C., Getzenberg, R. H., and Austin, R. H., 2010, “A microfluidic device for continuous cancer cell culture and passage with hydrodynamic forces.,” Lab Chip, **10**(14), pp. 1807–13.

[20] Liu, W., Li, L., Wang, X., Ren, L., Wang, X., Wang, J., Tu, Q., Huang, X., and Wang, J., 2010, “An integrated microfluidic system for studying cell-microenvironmental interactions versatilely and dynamically.,” Lab Chip, **10**(13), pp. 1717–24.

[21] Song, J. W., Gu, W., Futai, N., Warner, K. A., Nor, J. E., and Takayama, S., 2005, “Computer-controlled microcirculatory support system for endothelial cell culture and shearing.,” Anal. Chem., **77**(13), pp. 3993–9.

[22] Shao, J., Wu, L., Wu, J., Zheng, Y., Zhao, H., Jin, Q., and Zhao, J., 2009, “Integrated microfluidic chip for endothelial cells culture and analysis exposed to a pulsatile and oscillatory shear stress.,” Lab Chip, **9**(21), pp. 3118–25.

[23] Giridharan, G. A., Nguyen, M.-D., Estrada, R., Parichehreh, V., Hamid, T., Ismahil, M. A., Prabhu, S. D., and Sethu, P., 2010, “Microfluidic cardiac cell culture model (μCCCM).,” Anal. Chem., **82**(18), pp. 7581–7.

[24] Estrada, R., Giridharan, G. A., Nguyen, M.-D., Roussel, T. J., Shakeri, M., Parichehreh, V., Prabhu, S. D., and Sethu, P., 2011, “Endothelial cell culture model for replication of physiological profiles of pressure, flow, stretch, and shear stress in vitro.,” Anal. Chem., **83**(8), pp. 3170–7.

[25] VanDersarl, J. J., Xu, A. M., and Melosh, N. A., 2011, “Rapid spatial and temporal controlled signal delivery over large cell culture areas.,” Lab Chip, **11**(18), pp. 3057–63.

[26] Kawada, J., Kimura, H., Akutsu, H., Sakai, Y., and Fujii, T., 2012, “Spatiotemporally controlled delivery of soluble factors for stem cell differentiation.,” Lab Chip, **12**(21), pp. 4508–15.

[27] Wang, H.-Y., Bao, N., and Lu, C., 2008, “A microfluidic cell array with individually addressable culture chambers.,” Biosens. Bioelectron., **24**(4), pp. 613–7.

[28] Lee, J., Cuddihy, M. J., and Kotov, N. A., 2008, “Three-dimensional cell culture matrices: state of the art.,” Tissue Eng. Part B. Rev., **14**(1), pp. 61–86.

[29] Tang, M. D., Golden, A. P., and Tien, J., 2003, “Molding of three-dimensional microstructures of gels.,” J. Am. Chem. Soc., **125**(43), pp. 12988–9.

[30] Wong, A. P., Perez-Castillejos, R., Christopher Love, J., and Whitesides, G. M., 2008, “Partitioning microfluidic channels with hydrogel to construct tunable 3-D cellular microenvironments.,” Biomaterials, **29**(12), pp. 1853–61.

[31] Huang, C. P., Lu, J., Seon, H., Lee, A. P., Flanagan, L. A., Kim, H.-Y., Putnam, A. J., and Jeon, N. L., 2009, “Engineering microscale cellular niches for three-dimensional multicellular co-cultures.,” Lab Chip, **9**(12), pp. 1740–8.

[32] Frisk, T., Rydholm, S., Andersson, H., Stemme, G., and Brismar, H., 2005, “A concept for miniaturized 3-D cell culture using an extracellular matrix gel.,” Electrophoresis, **26**(24), pp. 4751–8.

[33] Frisk, T., Rydholm, S., Liebmann, T., Svahn, H. A., Stemme, G., and Brismar, H., 2007, “A microfluidic device for parallel 3-D cell cultures in asymmetric environments.,” Electrophoresis, **28**(24), pp. 4705–12.

[34] Ng, C. P., and Pun, S. H., 2008, “A perfusable 3D cell-matrix tissue culture chamber for in situ evaluation of nanoparticle vehicle penetration and transport.,” Biotechnol. Bioeng., **99**(6), pp. 1490–501.

[35] Vickerman, V., Blundo, J., Chung, S., and Kamm, R., 2008, “Design, fabrication and implementation of a novel multi-parameter control microfluidic platform for three-dimensional cell culture and real-time imaging.,” Lab Chip, **8**(9), pp. 1468–77.

[36] Chen, M. C. W., Gupta, M., and Cheung, K. C., 2010, “Alginate-based microfluidic system for tumor spheroid formation and anticancer agent screening.,” Biomed. Microdevices, **12**(4), pp. 647–54.

[37] Kim, M. S., Yeon, J. H., and Park, J.-K., 2007, “A microfluidic platform for 3-dimensional cell culture and cell-based assays.,” Biomed. Microdevices, **9**(1), pp. 25–34.

[38] Lii, J., Hsu, W.-J., Parsa, H., Das, A., Rouse, R., and Sia, S. K., 2008, “Real-time microfluidic system for studying mammalian cells in 3D microenvironments.,” Anal. Chem., **80**(10), pp. 3640–7.

[39] Toh, Y.-C., Zhang, C., Zhang, J., Khong, Y. M., Chang, S., Samper, V. D., van Noort, D., Hutmacher, D. W., and Yu, H., 2007, “A novel 3D mammalian cell perfusion-culture system in microfluidic channels.,” Lab Chip, **7**(3), pp. 302–9.

[40] Ong, S.-M., Zhang, C., Toh, Y.-C., Kim, S. H., Foo, H. L., Tan, C. H., van Noort, D., Park, S., and Yu, H., 2008, “A gel-free 3D microfluidic cell culture system.,” Biomaterials, **29**(22), pp. 3237–44.

[41] Toh, Y.-C., Lim, T. C., Tai, D., Xiao, G., van Noort, D., and Yu, H., 2009, “A microfluidic 3D hepatocyte chip for drug toxicity testing.,” Lab Chip, **9**(14), pp. 2026–35.

[42] Goral, V. N., Hsieh, Y.-C., Petzold, O. N., Clark, J. S., Yuen, P. K., and Faris, R. a, 2010, “Perfusion-based microfluidic device for three-dimensional dynamic primary human hepatocyte cell culture in the absence of biological or synthetic matrices or coagulants.,” Lab Chip, **10**(24), pp. 3380–6.

[43] Agastin, S., Giang, U.-B. T., Geng, Y., Delouise, L. A., and King, M. R., 2011, “Continuously perfused microbubble array for 3D tumor spheroid model.,” Biomicrofluidics, **5**(2), p. 24110.

[44] Ziółkowska, K., Stelmachowska, A., Kwapiszewski, R., Chudy, M., Dybko, A., and Brzózka, Z., 2012, “Long-term three-dimensional cell culture and anticancer drug activity evaluation in a microfluidic chip.,” Biosens. Bioelectron.

[45] Ota, H., and Miki, N., 2011, “Microfluidic experimental platform for producing size-controlled three-dimensional spheroids,” Sensors Actuators A Phys., **169**(2), pp. 266–273.

[46] Moon, H., Cho, S. K., Garrell, R. L., and Kim, C.-J. “CJ,” 2002, “Low voltage electrowetting-on-dielectric,” J. Appl. Phys., **92**(7), p. 4080.

[47] Pollack, M. G., Fair, R. B., and Shenderov, A. D., 2000, “Electrowetting-based actuation of liquid droplets for microfluidic applications,” Appl. Phys. Lett., **77**(11), p. 1725.

[48] Quilliet, C., and Berge, B., 2001, “Electrowetting: a recent outbreak,” Curr. Opin. Colloid Interface Sci., **6**(1), pp. 34–39.

[49] Cho, S. K., Moon, H., and Kim, C.-J., 2003, “Creating, transporting, cutting, and merging liquid droplets by electrowetting-based actuation for digital microfluidic circuits,” J. Microelectromechanical Syst., **12**(1), pp. 70–80.

[50] Ding, H., Sadeghi, S., Shah, G. J., Chen, S., Keng, P. Y., Kim, C.-J. C. J., and van Dam, R. M., 2012, “Accurate dispensing of volatile reagents on demand for chemical reactions in EWOD chips.,” Lab Chip, **12**(18), pp. 3331–40.

[51] Miller, E. M., and Wheeler, A. R., 2008, “A digital microfluidic approach to homogeneous enzyme assays.,” Anal. Chem., **80**(5), pp. 1614–9.

[52] Sista, R. S., Eckhardt, A. E., Srinivasan, V., Pollack, M. G., Palanki, S., and Pamula, V. K., 2008, “Heterogeneous immunoassays using magnetic beads on a digital microfluidic platform.,” Lab Chip, **8**(12), pp. 2188–96.

[53] Miller, E. M., Ng, A. H. C., Uddayasankar, U., and Wheeler, A. R., 2011, “A digital microfluidic approach to heterogeneous immunoassays.,” Anal. Bioanal. Chem., **399**(1), pp. 337–45.

[54] Ng, A. H. C., Choi, K., Luoma, R. P., Robinson, J. M., and Wheeler, A. R., 2012, “Digital microfluidic magnetic separation for particle-based immunoassays.,” Anal. Chem., **84**(20), pp. 8805–12.

[55] Chang, Y.-H., Lee, G.-B., Huang, F.-C., Chen, Y.-Y., and Lin, J.-L., 2006, “Integrated polymerase chain reaction chips utilizing digital microfluidics.,” Biomed. Microdevices, **8**(3), pp. 215–25.

[56] Hua, Z., Rouse, J. L., Eckhardt, A. E., Srinivasan, V., Pamula, V. K., Schell, W. A., Benton, J. L., Mitchell, T. G., and Pollack, M. G., 2010, “Multiplexed real-time polymerase chain reaction on a digital microfluidic platform.,” Anal. Chem., **82**(6), pp. 2310–6.

[57] Mousa, N. A., Jebrail, M. J., Yang, H., Abdelgawad, M., Metalnikov, P., Chen, J., Wheeler, A. R., and Casper, R. F., 2009, “Droplet-scale estrogen assays in breast tissue, blood, and serum.,” Sci. Transl. Med., **1**(1), p. 1ra2.

[58] Shih, S. C. C., Yang, H., Jebrail, M. J., Fobel, R., McIntosh, N., Al-Dirbashi, O. Y., Chakraborty, P., and Wheeler, A. R., 2012, “Dried blood spot analysis by digital microfluidics coupled to nanoelectrospray ionization mass spectrometry.,” Anal. Chem., **84**(8), pp. 3731–8.

[59] Wheeler, A. R., Moon, H., Kim, C.-J., Loo, J. A., and Garrell, R. L., 2004, “Electrowetting-based microfluidics for analysis of peptides and proteins by matrix-assisted laser desorption/ionization mass spectrometry.,” Anal. Chem., **76**(16), pp. 4833–8.

[60] Wheeler, A. R., Moon, H., Bird, C. A., Loo, R. R. O., Kim, C.-J. C. J., Loo, J. A., and Garrell, R. L., 2005, “Digital microfluidics with in-line sample purification for proteomics analyses with MALDI-MS.,” Anal. Chem., **77**(2), pp. 534–40.

[61] Jebrail, M. J., and Wheeler, A. R., 2009, “Digital microfluidic method for protein extraction by precipitation.,” Anal. Chem., **81**(1), pp. 330–5.

[62] Luk, V. N., and Wheeler, A. R., 2009, “A digital microfluidic approach to proteomic sample processing.,” Anal. Chem., **81**(11), pp. 4524–30.

[63] Sugiura, S., Sakai, Y., Nakazawa, K., and Kanamori, T., 2011, “Superior oxygen and glucose supply in perfusion cell cultures compared to static cell cultures demonstrated by simulations using the finite element method.,” Biomicrofluidics, **5**(2), p. 22202.

[64] Srinivasan, V., Pamula, V. K., and Fair, R. B., 2004, “An integrated digital microfluidic lab-on-a-chip for clinical diagnostics on human physiological fluids.,” Lab Chip, **4**(4), pp. 310–5.

[65] Luk, V. N., Mo, G. C., and Wheeler, A. R., 2008, “Pluronic additives: a solution to sticky problems in digital microfluidics.,” Langmuir, **24**(12), pp. 6382–9.

[66] Au, S. H., Kumar, P., and Wheeler, A. R., 2011, “A new angle on pluronic additives: advancing droplets and understanding in digital microfluidics.,” Langmuir, **27**(13), pp. 8586–94.

[67] Barbulovic-Nad, I., Yang, H., Park, P. S., and Wheeler, A. R., 2008, “Digital microfluidics for cell-based assays.,” Lab Chip, **8**(4), pp. 519–26.

[68] Son, S. U., and Garrell, R. L., 2009, “Transport of live yeast and zebrafish embryo on a droplet digital microfluidic platform.,” Lab Chip, **9**(16), pp. 2398–401.

[69] Au, S. H., Shih, S. C. C., and Wheeler, A. R., 2011, “Integrated microbioreactor for culture and analysis of bacteria, algae and yeast.,” Biomed. Microdevices, **13**(1), pp. 41–50.

[70] Barbulovic-Nad, I., Au, S. H., and Wheeler, A. R., 2010, “A microfluidic platform for complete mammalian cell culture.,” Lab Chip, **10**(12), pp. 1536–42.

[71] Srigunapalan, S., Eydelnant, I. A., Simmons, C. A., and Wheeler, A. R., 2012, “A digital microfluidic platform for primary cell culture and analysis.,” Lab Chip, **12**(2), pp. 369–75.

[72] Witters, D., Vergauwe, N., Vermeir, S., Ceyssens, F., Liekens, S., Puers, R., and Lammertyn, J., 2011, “Biofunctionalization of electrowetting-on-dielectric digital microfluidic chips for miniaturized cell-based applications.,” Lab Chip, **11**(16), pp. 2790–4.

[73] Eydelnant, I. A., Uddayasankar, U., Li, B., Liao, M. W., and Wheeler, A. R., 2012, “Virtual microwells for digital microfluidic reagent dispensing and cell culture.,” Lab Chip, **12**(4), pp. 750–7.

[74] Shih, S. C. C., Barbulovic-Nad, I., Yang, X., Fobel, R., and Wheeler, A. R., 2012, “Digital microfluidics with impedance sensing for integrated cell culture and analysis,” Biosens. Bioelectron., **null**(null).

[75] Shah, G. J., Veale, J. L., Korin, Y., Reed, E. F., Gritsch, H. A., and Kim, C.-J. C., 2010, “Specific binding and magnetic concentration of CD8+ T-lymphocytes on electrowetting-on-dielectric platform.,” Biomicrofluidics, **4**(4), p. 44106.

[76] Vergauwe, N., Witters, D., Ceyssens, F., Vermeir, S., Verbruggen, B., Puers, R., and Lammertyn, J., 2011, “A versatile electrowetting-based digital microfluidic platform for quantitative homogeneous and heterogeneous bio-assays,” J. Micromechanics Microengineering, **21**(5), p. 054026.

[77] Bogojevic, D., Chamberlain, M. D., Barbulovic-Nad, I., and Wheeler, A. R., 2012, “A digital microfluidic method for multiplexed cell-based apoptosis assays.,” Lab Chip, **12**(3), pp. 627–34.

[78] Park, S., Wijethunga, P. A. L., Moon, H., and Han, B., 2011, “On-chip characterization of cryoprotective agent mixtures using an EWOD-based digital microfluidic device.,” Lab Chip, **11**(13), pp. 2212–21.

[79] George, S. M., and Moon, H., 2011, “Digital Microfluidic Platform for 3-D Tissue Based High Throughput Screening,” ASME 2011 Summer Bioengineering Conference, Parts A and B, ASME, p. 105.

[80] George, S. M., and Moon, H., 2011, “Three Dimensional Tissue Based Digital Microfluidic Screening Platform,” 15th International Conference on Miniaturized Systems for Chemistry and Life Sciences (μTAS), Seattle.

[81] Fiddes, L. K., Luk, V. N., Au, S. H., Ng, A. H. C., Luk, V., Kumacheva, E., and Wheeler, A. R., 2012, “Hydrogel discs for digital microfluidics.,” Biomicrofluidics, **6**(1), pp. 14112–1411211.

[82] Eydelnant, I. A., Betty Li, B., and Wheeler, A. R., 2014, “Microgels on-demand.,” Nat. Commun., **5**, p. 3355.

[83] Au, S. H., Chamberlain, M. D., Mahesh, S., Sefton, M. V, and Wheeler, A. R., 2014, “Hepatic organoids for microfluidic drug screening.,” Lab Chip, **14**(17), pp. 3290–9.

[84] Choi, N. W., Cabodi, M., Held, B., Gleghorn, J. P., Bonassar, L. J., and Stroock, A. D., 2007, “Microfluidic scaffolds for tissue engineering.,” Nat. Mater., **6**(11), pp. 908–15.

[85] Lee, K. Y., and Mooney, D. J., 2001, “Hydrogels for Tissue Engineering,” Chem. Rev., **101**(7), pp. 1869–1880.

[86] Kuo, C. K., and Ma, P. X., 2001, “Ionically crosslinked alginate hydrogels as scaffolds for tissue engineering: part 1. Structure, gelation rate and mechanical properties.,” Biomaterials, **22**(6), pp. 511–21.

[87] Orive, G., Ponce, S., Hernández, R. ., Gascón, A. ., Igartua, M., and Pedraz, J. ., 2002, “Biocompatibility of microcapsules for cell immobilization elaborated with different type of alginates,” Biomaterials, **23**(18), pp. 3825–3831.

[88] Braschler, T., Johann, R., Heule, M., Metref, L., and Renaud, P., 2005, “Gentle cell trapping and release on a microfluidic chip by in situ alginate hydrogel formation.,” Lab Chip, **5**(5), pp. 553–9.

[89] Manojlovic, V., Djonlagic, J., Obradovic, B., Nedovic, V., and Bugarski, B., 2006, “Investigations of cell immobilization in alginate: rheological and electrostatic extrusion studies,” J. Chem. Technol. Biotechnol., **81**(4), pp. 505–510.

[90] Rowley, J. A., Madlambayan, G., and Mooney, D. J., 1999, “Alginate hydrogels as synthetic extracellular matrix materials,” Biomaterials, **20**(1), pp. 45–53.

[91] Augst, A. D., Kong, H. J., and Mooney, D. J., 2006, “Alginate hydrogels as biomaterials.,” Macromol. Biosci., **6**(8), pp. 623–33.

[92] Martinez, C. J., Kim, J. W., Ye, C., Ortiz, I., Rowat, A. C., Marquez, M., and Weitz, D., 2012, “A microfluidic approach to encapsulate living cells in uniform alginate hydrogel microparticles.,” Macromol. Biosci., **12**(7), pp. 946–51.

[93] Choi, C.-H., Jung, J.-H., Rhee, Y. W., Kim, D.-P., Shim, S.-E., and Lee, C.-S., 2007, “Generation of monodisperse alginate microbeads and in situ encapsulation of cell in microfluidic device.,” Biomed. Microdevices, **9**(6), pp. 855–62.

[94] Yu, L., Chen, M. C. W., and Cheung, K. C., 2010, “Droplet-based microfluidic system for multicellular tumor spheroid formation and anticancer drug testing.,” Lab Chip, **10**(18), pp. 2424–32.

[95] Wong, A. P., Perez-Castillejos, R., Christopher Love, J., and Whitesides, G. M., 2008, “Partitioning microfluidic channels with hydrogel to construct tunable 3-D cellular microenvironments.,” Biomaterials, **29**(12), pp. 1853–61.

[96] Johann, R. M., and Renaud, P., 2007, “Microfluidic patterning of alginate hydrogels.,” Biointerphases, **2**(2), pp. 73–9.

[97] Lee, M.-Y., Kumar, R. A., Sukumaran, S. M., Hogg, M. G., Clark, D. S., and Dordick, J. S., 2008, “Three-dimensional cellular microarray for high-throughput toxicology assays.,” Proc. Natl. Acad. Sci. U. S. A., **105**(1), pp. 59–63.

[98] Inoue, S. K., 1997, “A moving boundary model of calcium alginate gel formation and the estimation of diffusion and mass transfer coefficients.”

[99] Braschler, T., Valero, A., Colella, L., Pataky, K., Brugger, J., and Renaud, P., 2011, “Link between alginate reaction front propagation and general reaction diffusion theory.,” Anal. Chem., **83**(6), pp. 2234–42.

[100] Fang, Y., Al-Assaf, S., Phillips, G. O., Nishinari, K., Funami, T., Williams, P. A., and Li, L., 2007, “Multiple steps and critical behaviors of the binding of calcium to alginate.,” J. Phys. Chem. B, **111**(10), pp. 2456–62.

[101] Borgogna, M., Skjåk-Bræk, G., Paoletti, S., and Donati, I., 2013, “On the initial binding of alginate by calcium ions. The tilted egg-box hypothesis.,” J. Phys. Chem. B, **117**(24), pp. 7277–82.

[102] Eydelnant, I. A., Uddayasankar, U., Li, B., Liao, M. W., and Wheeler, A. R., 2012, “Virtual microwells for digital microfluidic reagent dispensing and cell culture.,” Lab Chip, **12**(4), pp. 750–7.

[103] Lu, H.-W., Glasner, K., Bertozzi, A. L., and Kim, C.-J., 2007, “A diffuse-interface model for electrowetting drops in a Hele-Shaw cell,” J. Fluid Mech., **590**, pp. 411–435.

[104] Nikapitiya, J. Y., 2013, “Study of the capabilities of electrowetting on dielectric digital microfluidics (EWOD DMF) towards the high efficient thin-film evaporative cooling platform,” University of Texas at Arlington.

Biographical Information

Subin George obtained his Bachelor of Technology degree in Mechanical Engineering from the University of Kerala, India in May 2005. He then went on to pursue his Master of Science in Mechanical Engineering from the University of Michigan, Ann Arbor, graduating in May 2007 with a focus on product design. After realizing his interest in biomedical applications within mechanical engineering, he came to the University of Texas at Arlington where he carried out work for his doctorate degree in Mechanical Engineering with a focus on bio-MEMS and microfluidics. His current research interests revolve around the applications of mechanical engineering for biomedical applications and are specifically focused on the development of lab on a chip devices.